


# Simulating Binary Evolution Using Population Synthesis Suite COSMIC to Explore Neutron Star High-Mass X-Ray Binary Peculiar Velocities

Harry P. Johnson<sup>1</sup>  Supervisor - Poshak Gandhi,<sup>1</sup> Module Code - PHYS6006<sup>1</sup>

<sup>1</sup>University of Southampton, University Road, Southampton SO17 1BJ, UK

21 August 2025

## ABSTRACT

Neutron stars (NSs) in a neutron star high-mass x-ray binary (NS HMXBs) will have all undergone a supernova and possibly impart a large peculiar velocity onto the binary via a natal kick. Using the most recent data release from the *Gaia* mission, DR3, and data from previous literature, I calculate such peculiar velocities for 16 such NS HMXBs with known companion mass. I find a result of increasing peculiar velocity with companion mass, having a Pearson's R of 0.504 which is accepted at the 5% confidence interval. I then move onto using the COSMIC binary synthesis suite to try and recreate this result in simulation. After using multiple kick prescriptions and exploring the mass and period parameter spaces for the binaries, I fail to recreate the correlation. This calls for further research into the dynamics of binary evolution.

Word Count - 7452

## 1 INTRODUCTION

Neutron stars (NSs) are one of the many possible outcomes of stellar evolution. At the end of a heavy stars life (typically  $\geq 9M_{\odot}$ , [Sukhbold et al. \(2016\)](#)) it will undergo supernova and result in either a neutron star, black hole, or possibly not survive the explosion. [Heger et al. \(2003\)](#) give an excellent summary of the different types of supernova, and what the possible remnants are dependant on the mass and metallicity of the progenitor star. Supernova are inherently violent events which release mass amounts of energy. A typical O class star can release  $\approx 10^{44}J$  of energy in the instant of a supernova explosion, which is a substantial fraction of the  $\approx 10^{45}J$  it could emit up to that point, during a typical lifetime of  $5Myr$  ([Walch & Naab \(2015\)](#)). This energy is released mostly via the neutrinos formed in the explosion, however some is taken away in the launched stellar atmosphere in which more nuclear fusion may occur, giving the bright appearance of the supernova.

It is known that newly formed neutron stars (which we commonly observe as pulsars, [Stappers et al. \(2011\)](#)) can be moving at blistering speeds, typically of the order of  $100kms^{-1}$  and in rare cases, possibly up to  $1000kms^{-1}$ , [Hobbs et al. \(2005\)](#). The explanation of these velocities is a kick at birth from the supernova, a so called natal/asymmetric kick. The mechanism behind these kicks is poorly understood at present with many possible theories as to why they may occur (see a summary by [Lai \(2001\)](#)).

A natural extension to considering the impact of kicks for single star systems is to consider binary systems. After all, binary systems make up a substantial fraction of all stellar systems. A type of system known as an x-ray binary (XRB) provide excellent grounds for study of the impact of kicks on binaries, as they must contain a compact object (either a black hole or neutron star) and a main sequence companion which donates mass to the compact object, allowing it to shine brightly in the x-ray. We split these x-ray binaries first into 2 categories, based on the mass of the companion star. For companion masses of  $M \geq 8M_{\odot}$  we denote high-mass x-ray binaries (HMXBs)

and for lower masses low-mass x-ray binaries (LMXBs). A further distinguishing factor is whether the system hosts a NS or black hole (BH). This work focuses on NS HMXBs, or high-mass x-ray binaries that have a neutron star companion. Naturally we may even further split the systems based on the class of companion star. For instance, it might be useful to specifically talk about Be class companions, or perhaps supergiant (sg) companions as their methods of mass transfer are different (see reviews by [Rivinius et al. \(2013\)](#) and [Chaty \(2013\)](#) respectively). In this work, I do not distinguish between these systems however.

A natal kick is a key event in the evolution of a binary and can have a massive effect on its orbital parameters and overall velocity, as explored by [Brandt & Podsiadlowski \(1995\)](#). An excellent understanding of the impacts of these kicks could help improve our understanding and answer questions of HMXB evolution - Where and how do these systems form? Of course, natal kicks are also intrinsically linked to the supernova mechanism and so a better understanding of kicks might bring new insights to whether supernova kicks are more neutrino or ejecta driven, [Fryer & Kusenko \(2006\)](#).

A number of our models for kicks are based on the physics and observations of single stars. [Hobbs et al. \(2005\)](#) found that kicks can be modelled as a maxwellian distribution with a dispersion of  $265kms^{-1}$  from observations of pulsars. Observations of the spin and proper motions of pulsars also indicate that kicks might be preferentially directed along or near the spin axis of the object, shown by [Wang et al. \(2006\)](#), [Ng & Romani \(2007\)](#), and [Kaplan et al. \(2008\)](#). From here, adjustments may be made to include new physics. For instance, [Fryer et al. \(2012\)](#) detail 2 new prescriptions for the supernova. Both account for possible mass falling back onto the exploding star. The differences arise from the time between core bounce and supernova - one method allows for only rapid explosions with a time difference of up to  $250ms$ , and the other allows for more delayed explosions.

In this project, I aim to test some such kick models against data from known NS HMXB systems. For this, I require high quality binary parameters to allow for calculation of systemic velocities, along with companion masses for my systems. The *Gaia* satellite ([Gaia Collaboration et al. \(2016\)](#)) provides and its recent data release, DR3,

(Gaia Collaboration et al. (2022)) provides high quality astrometric parameters (full 3D positions using parallax, and 2D proper motions in the plane of the sky) that I may use to calculate peculiar velocities. The final required parameters (radial velocities and companion masses) come from the literature. After calculating the peculiar velocities for a group of systems, I use the COSMIC binary synthesis suite (Breivik et al. (2020a)) to simulate many HMXB systems over the mass and period parameter space to see if our current models match what we observe.

In section 2 I start by gathering a list of known NS HMXBs from the literature and finding their counterparts in *Gaia* DR3. Next, in section 3 I compute the peculiar velocities and uncertainties of my systems. After this, I introduce COSMIC and outline my methodology for simulating many HMXB systems over the mass and orbital period parameter spaces in section 4. In sections 5 and 6 I present my results and provide discussion before finally concluding in section 7.

## 2 DATA COMPILATION

### 2.1 Methodology

In this section I gather data on a variety of HMXB systems. I use the catalogue compiled by Fortin et al. (2022), and filter out any unwanted systems. I then find the counterparts in *Gaia* DR3, using SIMBAD to assist with the cross-matching as Fortin et al. (2022) used *Gaia* EDR3. The final data is then taken from both *Gaia* and the literature, with proper motions (2D) and full 3D coordinates from *Gaia*, and radial velocities + companion masses from the literature.

### 2.2 HMXB Sample

The *Gaia* database does not include data on whether a star system is an HMXB, therefore I have to rely on previous literature for my sample. This work uses the systems compiled by Fortin et al. (2022), all of which are NS (Neutron Star) HMXBs, systems having a NS compact object. I took a subset of the systems compiled within, only ones which have explicit values of the radial velocity and companion mass. This leaves me with 17 potential systems, of which I use 16. The final exclusion is explained in section 2.4. *Gaia* does not contain information on companion masses, and while the satellite does have the capability to measure radial velocities from spectra it is a rarity for a specific system to have this measured. None of the systems in the set I used have radial velocities in *Gaia*.

### 2.3 Querying *Gaia*

Since Fortin et al. (2022) use *Gaia* EDR3 for their data, I need to find the correct systems in the newer *Gaia* DR3 data set. The unique IDs between the two data sets are different, so I manually cross-matched the systems using the SIMBAD database (Wenger et al. (2000)), so that I could find the correct DR3 source IDs with absolute certainty. I then simply created my own table which contained the source IDs, then performed an inner join with *Gaia* DR3. The query I used can be seen in appendix A.

### 2.4 The Final Sample

After collecting the data on the 17 systems, I performed a final look over the data to remove any unsuitable systems. I chose to remove system 2FGL J1019.0-5856 from the sample due to its high fractional parallax error of  $\approx 80\%$ . It is known that using parallax inversion

(equation 1) to calculate distances when fractional error is large is inaccurate, as shown by Bailer-Jones (2015). A more accurate calculation would include using Bayesian statistics, a method outlined in Bailer-Jones et al. (2021). Due to the high complexity of this approach, I decided to exclude the offending system and use simple parallax inversion.

$$d = \frac{1}{\pi} \quad (1)$$

Where  $d$  is the distance in parsecs and  $\pi$  is the parallax in arc seconds.

## 2.5 Data Tables

Tables 1 and 2 show the data values collected from literature and *Gaia* respectively.

## 3 PECULIAR VELOCITIES

### 3.1 Calculating Peculiar Velocity

The total velocity of the systems is not only composed of their peculiar velocities. These extra sources of velocity need to be removed - velocity due to rotation around the galactic centre, and apparent velocity due to the motion of the Sun. In addition, the proper motions from *Gaia* need to be converted from Ra Dec coordinates to galactic coordinates. The python module Astropy (Astropy Collaboration et al. (2022)) provides a convenient method of conversion from Ra Dec to galactic. Numerous constants are needed for the conversion, I used  $R_{\odot} = 8.2$  kpc for the distance to the galactic centre,  $v_{LSR} = 236$   $\text{km s}^{-1}$  for the galactic rotation speed, and  $v_{\odot} = (8.0, 12.4, 7.7)$  for the solar velocity, all following Kawata et al. (2019). In addition, I used a height of 27pc for the Sun's height above the galactic plane following Chen et al. (2001). Once converting my velocities to the galactocentric frame using Astropy, I follow the appendix of Reid et al. (2009) to remove the undesired components of velocity. The last step for the total velocity is simply Pythagorean velocity addition. Appendix B shows my exact method.

### 3.2 Galactic Potential

A more accurate treatment would involve using the galactic potential for galactic rotation velocity as in reality it is not constant with distance. Mróz et al. (2019) calculate a galactic rotation curve using Cepheid variables and find that the rotation curve is almost flat for radii between  $4 \lesssim R \lesssim 20$  kpc. In table 3 I calculate the radii of the systems relative to the galactic centre in my sample using the parameters mentioned in section 3.1. They all lie within the range of  $4 \lesssim R \lesssim 20$  kpc, so my usage of a constant galactic rotation velocity is suitable.

### 3.3 Uncertainty Propagation

The conversion from proper motion and radial velocity to peculiar velocity is complex, and thus Monte Carlo uncertainty propagation is appropriate. I generated 50000 values of the peculiar velocity for each system, assuming all uncertainties are Gaussian to produce a probability density function (PDF) from which I may calculate the mean and standard deviation, along with the median and surrounding  $1-\sigma$  uncertainty. I ensured that no nonphysical values for any quantities were generated, in particular negative parallaxes. It is possible to use negative parallax values with a more robust method of estimating

**Table 1.** Literature values for the HMXBs. For systems without a given mass error, a systematic error of 20% will be used. The mean literature error is approximately 20%, so this is a reasonable assumption. My calculated peculiar velocities are given as both the mean and standard deviation, along with the median and surrounding  $1-\sigma$  area.

Name	DR3 ID	Type	Spectral Type	Ref	Companion Mass $M_{\odot}$	Ref	Radial Velocity $\text{km s}^{-1}$	Ref	Median Pv $\text{km s}^{-1}$	Mean Pv $\text{km s}^{-1}$
IGR J00370+6122	427234969757165952	Be	B0.5II-III	[1]	22.0	[2]	$-80.0 \pm 3.0$	[2]	$29.8^{+3.3}_{-3.3}$	$29.8 \pm 3.3$
1A 0114+650	524924310153249920	sg	B1Iae	[3]	$16.0 \pm 2.0$	[4]	$-31.0 \pm 5.0$	[5]	$41.6^{+5.0}_{-4.7}$	$41.8 \pm 4.8$
LS I+61 303	465645515129855872	Be	B0Ve	[6]	12.5	[7]	$41.4 \pm 0.6$	[8]	$10.6^{+0.3}_{-0.3}$	$10.6 \pm 0.3$
X Per	168450545792009600	Be	O9.5III	[9]	15.5	[10]	$1.0 \pm 0.9$	[11]	$12.1^{+0.2}_{-0.2}$	$12.1 \pm 0.2$
1A 0535+262	3441207615229815040	Oe	O9.5III-Ve	[12]	20.0	[13]	$-30.0 \pm 4.0$	[14]	$41.9^{+3.9}_{-3.8}$	$41.9 \pm 3.8$
HD 259440	3131822364779745536	Be	B0pe	[15]	$15.7 \pm 2.5$	[16]	$39.6 \pm 0.8$	[17]	$8.9^{+0.7}_{-0.7}$	$8.9 \pm 0.7$
IGR J08408-4503	5522306019626566528	sg	O8.5Ib-II(f)p	[18]	33.0	[19]	$15.3 \pm 0.5$	[19]	$40.0^{+2.2}_{-2.1}$	$40.0 \pm 2.2$
Vela X-1	5620657678322625920	sg	B0.5Iae-1b	[20]	$26.0 \pm 1.0$	[21]	$-3.2 \pm 0.9$	[22]	$58.0^{+1.8}_{-1.7}$	$58.0 \pm 1.8$
1E 1145.1-6141	5334851450481641088	sg	B2Iae	[23]	$14.0 \pm 4.0$	[24]	$-13.0 \pm 3.0$	[24]	$49.8^{+10.0}_{-7.3}$	$51.2 \pm 9.1$
GX 301-2	6054569565614460800	sg	B1.5Iaeq	[25]	$43.0 \pm 10.0$	[26]	$4.1 \pm 2.4$	[26]	$59.7^{+3.9}_{-3.6}$	$59.9 \pm 3.7$
PSR B1259-63	5862299960127967488	Oe	O9.5Ve	[27]	$22.0 \pm 7.5$	[28]	$0.0 \pm 1.0$	[29]	$24.3^{+1.1}_{-1.1}$	$24.3 \pm 1.1$
4U 1538-522	5886085557746480000	sg	B0.2Ia	[30]	20.0	[31]	$-158.0 \pm 11.0$	[31]	$73.9^{+12.7}_{-9.4}$	$76.1 \pm 13.6$
4U 1700-377	5976382915813535232	sg	O6Iafcp	[18]	$46.0 \pm 5.0$	[21]	$-60.0 \pm 10.0$	[32]	$73.6^{+6.3}_{-5.5}$	$74.0 \pm 5.9$
IGR J17544-2619	4063908810076415872	sg	O9Ib	[33]	$23.0 \pm 2.0$	[34]	$-46.8 \pm 4.0$	[35]	$45.1^{+4.0}_{-3.9}$	$45.1 \pm 3.9$
LS5039	4104196427943626624	Oe	ON6.5V(f)	[36]	23.0	[37]	$17.3 \pm 0.5$	[38]	$95.1^{+3.2}_{-3.0}$	$95.2 \pm 3.1$
4U 2206+543	2005653524280214400	Oe	O9.5Vep	[39]	18.0	[40]	$-54.5 \pm 1.0$	[41]	$22.1^{+0.8}_{-0.7}$	$22.8 \pm 0.8$

**References.** [1] Reig et al. (2005); [2] Grunhut et al. (2014); [3] Krtićka et al. (2015); [4] Hu et al. (2017); [5] Koenigsberger et al. (2003); [6] Hutchings et al. (1981); [7] Casares et al. (2005a); [8] Aragona et al. (2009); [9] Slettebak (1982); [10] Lyubimkov et al. (1997); [11] Grundstrom et al. (2007); [12] Wang & Gies (1998); [13] Okazaki & Negueruela (2001); [14] Hutchings (1984); [15] Jaschek & Egret (1982); [16] Aragona et al. (2010); [17] Moritani et al. (2018); [18] Sota et al. (2014); [19] Gamen et al. (2015); [20] Houk (1978); [21] Falanga et al. (2015); [22] Stickland et al. (1997); [23] Densham & Charles (1982); [24] Hutchings et al. (1987); [25] Hutchings et al. (1982); [26] Kaper et al. (2006); [27] Negueruela et al. (2011); [28] Miller-Jones et al. (2018); [29] Fortin et al. (2022); [30] Parkes et al. (1978); [31] Abubekrov et al. (2004); [32] Gies & Bolton (1986); [33] Pellizza et al. (2006); [34] Bikmaev et al. (2017); [35] Nikolaeva et al. (2013); [36] Townsend et al. (2011); [37] Casares et al. (2005b); [38] Casares et al. (2011); [39] Blay et al. (2006); [40] Zorec et al. (2005); [41] Stoyanov et al. (2014)

errors, an example of such is shown in Bailer-Jones et al. (2021). An example PDF for system IGR J00370+6122 is shown in figure 1.

### 3.4 Peculiar Velocity Against Companion Mass

Figure 2 shows the final plot of companion mass against peculiar velocity along with error bars. There is a moderate positive correlation with a Pearsons R of 0.504 that is statistically significant at the 5% confidence level, having a p-value of 0.046. This is a rather curious result, I would naively expect a negative correlation, due to more massive objects needing more imparted momentum to reach higher velocities. This result is discussed in section 6.

## 4 SIMULATIONS USING COSMIC

COSMIC Breivik et al. (2020a) is a binary synthesis suite, used to generate and evolve binaries. It implements evolutionary processes using BSE (Hurley et al. (2002)) with some updates pertaining to recent discoveries for binary evolution. These include metallicity dependant stellar winds, modifications to black hole kick strengths among others. While the software offers many options of customisation for different elements of binary evolution (winds, common envelope evolution, tides etc), I am only interested in the supernova

kicks. Therefore I left all configurations as default except for ones that directly involved kicks. Ideally, I would look into changing these other qualities and the effects of doing so, however they are complex and time consuming. A major limitation for this project is that of time - these simulations take a long time to run. This is discussed in section 5.7.

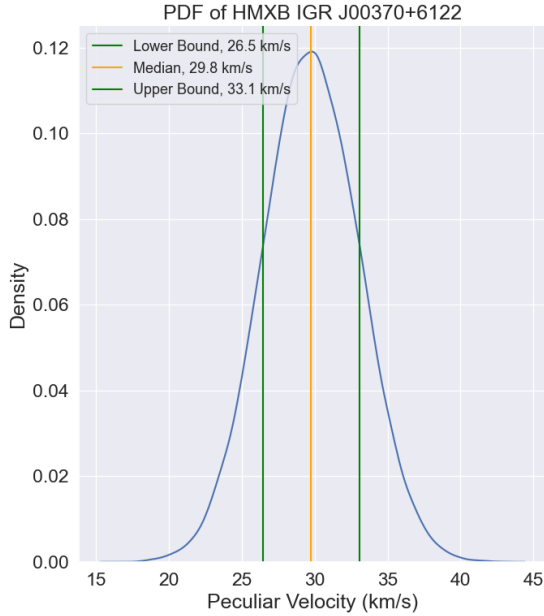
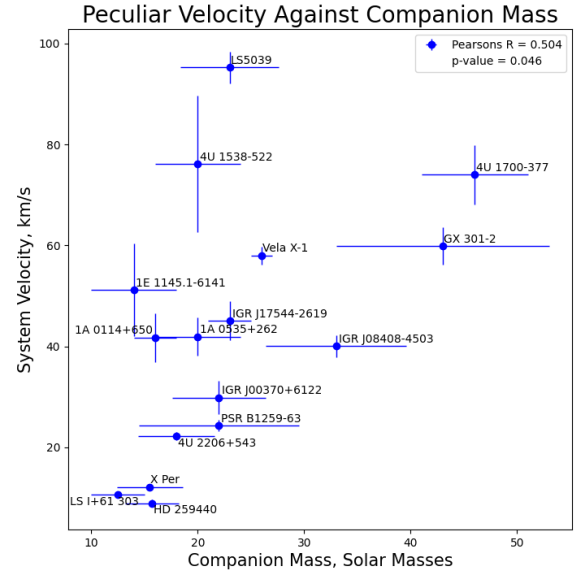
### 4.1 Kick Prescriptions

By default in COSMIC the kick velocities are pulled from a bimodal distribution, dependant on whether the supernova is an iron core collapse supernova (FeCCSN) or electron capture supernova/ultra stripped supernova (ECSN/USSN). The kick direction is also drawn isotropically. For FeCCSN, COSMIC uses a maxwellian distribution with a dispersion of  $\sigma = 265 \text{ km s}^{-1}$  following Hobbs et al. (2005). If the system undergoes an ECSN/USSN instead an alternate dispersion velocity is used, or the value used for the FeCCSN is divided by a factor of your choosing. I left this as its default value. Once the kick velocity is generated, it gets scaled based on how much mass falls back onto the compact object. A more detailed description can be seen in section 3.3 of COSMIC's accompanying paper, Breivik et al. (2020a).

2 alternate kick descriptions included within COSMIC that I tried simply use the maxwellian distribution of dispersion  $\sigma = 265 \text{ km s}^{-1}$

**Table 2.** Data taken from *Gaia* DR3, used to calculate the peculiar velocities of the HMXB star systems.

Name	DR3 ID	Right Ascension deg	Declination deg	RA Proper Motion mas yr <sup>-1</sup>	Dec Proper Motion mas yr <sup>-1</sup>	Parallax mas
IGR J00370+6122	427234969757165952	9.2901 ± 0.0084	61.3601 ± 0.0098	-1.7956 ± 0.0109	-0.5251 ± 0.0136	0.2719 ± 0.0121
1A 0114+650	524924310153249920	19.5112 ± 0.0075	65.2916 ± 0.0089	-1.2434 ± 0.0092	0.7606 ± 0.0118	0.1964 ± 0.0113
LS I+61 303	465645515129855872	40.1319 ± 0.0073	61.2293 ± 0.0092	-0.4234 ± 0.0113	-0.2555 ± 0.0119	0.3776 ± 0.0130
X Per	168450545792009600	58.8462 ± 0.0296	31.0458 ± 0.0208	-1.2821 ± 0.0531	-1.8691 ± 0.0303	1.6264 ± 0.0375
1A 0535+262	3441207615229815040	84.7274 ± 0.0203	26.3158 ± 0.0158	-0.5898 ± 0.0309	-2.8796 ± 0.0162	0.5245 ± 0.0233
HD 259440	3131822364779745536	98.2469 ± 0.0175	5.8003 ± 0.0163	-0.0259 ± 0.0201	-0.4284 ± 0.0162	0.5404 ± 0.0226
IGR J08408-4503	5522306019626566528	130.1991 ± 0.0142	-45.0584 ± 0.0142	-7.4647 ± 0.0196	6.0996 ± 0.0193	0.4430 ± 0.0168
Vela X-1	5620657678322625920	135.5286 ± 0.0109	-40.5547 ± 0.0127	-4.822 ± 0.0147	9.2817 ± 0.0162	0.4962 ± 0.0152
1E 1145.1-6141	5334851450481641088	176.8689 ± 0.0075	-61.9357 ± 0.0090	-6.2256 ± 0.0104	2.3615 ± 0.0199	0.1267 ± 0.0102
GX 301-2	6054569565614460800	186.6565 ± 0.0120	-62.7704 ± 0.0133	-5.2269 ± 0.0158	-2.0708 ± 0.0188	0.2506 ± 0.0160
PSR B1259-63	5862299960127967488	195.6985 ± 0.0089	-63.8357 ± 0.0100	-7.0928 ± 0.0118	-0.342 ± 0.0142	0.4434 ± 0.0133
4U 1538-522	5886085557746480000	235.5973 ± 0.0109	-52.3860 ± 0.0094	-6.7106 ± 0.0148	-4.1109 ± 0.0139	0.128 ± 0.0153
4U 1700-377	5976382915813535232	255.9866 ± 0.0210	-37.8441 ± 0.0121	2.4137 ± 0.0281	5.0219 ± 0.0213	0.6327 ± 0.0259
IGR J17544-2619	4063908810076415872	268.6053 ± 0.0222	-26.3313 ± 0.0173	-0.5057 ± 0.0286	-0.6678 ± 0.0182	0.3963 ± 0.0267
LS5039	4104196427943626624	276.5628 ± 0.0127	-14.8484 ± 0.0113	7.4253 ± 0.0142	-8.1512 ± 0.0117	0.4900 ± 0.0150
4U 2206+543	2005653524280214400	331.9843 ± 0.0121	54.5184 ± 0.0113	-4.1725 ± 0.0152	-3.3166 ± 0.0136	0.3051 ± 0.0136

**Figure 1.** Probability density function for the peculiar velocity of HMXB IGR J00370+6122.**Figure 2.** Peculiar Velocity (kms<sup>-1</sup>) against Companion Mass ( $M_{\odot}$ )

mentioned, but all kicks regardless of supernova type get scaled by the same factor.

Kick prescription A follows equation 1 from [Giacobbo & Mapelli \(2020\)](#), reproduced below in equation 2. Here, the kick velocity  $f$  generated from the distribution is scaled by the ejected mass ( $m_{ej}$ )

and remnant mass ( $m_{rem}$ ). The values of  $\langle m_{ej} \rangle$  and  $\langle m_{NS} \rangle$  are the average ejecta and neutron star masses respectively, taken to be  $9M_{\odot}$  and  $1.2M_{\odot}$ .

$$v_{kick} = f \frac{m_{ej}}{\langle m_{ej} \rangle} \frac{\langle m_{NS} \rangle}{m_{rem}} \quad (2)$$

**Table 3.** Distances to the galactic centre for the stars in the sample.

Name	DR3 ID	Galactic Centre Distance kpc
IGR J00370+6122	427234969757165952	$10.5891 \pm 0.1238$
1A 0114+650	524924310153249920	$11.9258 \pm 0.2462$
LS I+61 303	465645515129855872	$10.2646 \pm 0.0760$
X Per	168450545792009600	$8.7656 \pm 0.0132$
1A 0535+262	3441207615229815040	$10.1075 \pm 0.0849$
HD 259440	3131822364779745536	$9.9033 \pm 0.0731$
IGR J08408-4503	5522306019626566528	$8.7295 \pm 0.0308$
Vela X-1	5620657678322625920	$8.6777 \pm 0.0215$
1E 1145.1-6141	5334851450481641088	$8.6366 \pm 0.3452$
GX 301-2	6054569565614460800	$7.0999 \pm 0.0072$
PSR B1259-63	5862299960127967488	$7.1794 \pm 0.0222$
4U 1538-522	5886085557746480000	$4.6365 \pm 0.3127$
4U 1700-377	5976382915813535232	$6.6631 \pm 0.0629$
IGR J17544-2619	4063908810076415872	$5.6710 \pm 0.1723$
LS5039	4104196427943626624	$6.2740 \pm 0.0578$
4U 2206+543	2005653524280214400	$9.3784 \pm 0.0760$

Prescription B is also provided by [Giacobbo & Mapelli \(2020\)](#), equation 2 within. It is similar to prescription 1, however it is now independent of the remnant mass, and takes the form of equation 3.

$$v_{kick} = f \frac{m_{ej}}{\langle m_{ej} \rangle} \quad (3)$$

It should be noted that [Giacobbo & Mapelli \(2020\)](#) say that kick prescription A generates smaller kicks for more massive systems, which is the opposite of what I obtained in graph 2.

A final kick prescription is to simply remove the natal kick entirely. This still leaves the symmetric kick (as it is required via momentum conservation). A calculation of the symmetric kick velocity may be found in section 6 of [Blaauw \(1961\)](#).

The following list summarises the kick prescriptions that I will be testing -

- Default Kick. Bimodal Distribution. Maxwellian with dispersion of  $\sigma = 265 \text{ km s}^{-1}$  for FeCCSN. ECSN/USSN use a Maxwellian with a different dispersion, or the same as before but with sigma divided by a factor. Then the kick is scaled dependant on how much mass falls back onto the compact object.
- Kick A. Maxwellian with dispersion of  $\sigma = 265 \text{ km s}^{-1}$  scaled by the ejecta mass divided by the remnant mass and some constants, equation 2.
- Kick B. Maxwellian with dispersion of  $\sigma = 265 \text{ km s}^{-1}$  scaled by the ejecta mass and a constant only, equation 3.
- No Asymmetric Kicks. Only the kick due to mass loss and the resultant change in the location of the centre of mass is included.

## 4.2 Running the Simulations

### 4.2.1 Parameter Space

There are many parts of the parameter space that I could explore. I chose to explore a space including masses and orbital periods in the following combinations -

- Both the companion and progenitor masses.
- The companion mass and orbital period of the binary.

For each pair of parameters I wanted to test a variety of kick velocities. Since they are randomly generated, I simulated 50 systems for each pair.

For the simulations where I changed both masses, I had the progenitor mass range from  $30 \rightarrow 60 M_{\odot}$ , and the companion from  $20 M_{\odot}$  up to the current progenitor mass being simulated, both in steps of  $1 M_{\odot}$ . These large masses were used as I required my systems to evolve into HMXBs. Lower masses of course could still result in HMXBs, however increasing the range would drastically increase the simulation time which is necessary to avoid. For the periods, I chose a period length of 20 days, to keep these simulations somewhat comparable to the simulations in which I varied the period.

For the period-companion mass simulations, I kept the mass of the progenitor constant. I chose to use a mass of  $20 M_{\odot}$ , as a star of that mass undergoing supernova results in a neutron star a vast majority of the time. As a result, the maximum companion mass that I could use was  $20 M_{\odot}$ , to ensure that the progenitor goes supernova first. I chose to range it from  $5 \rightarrow 19.75 M_{\odot}$  in  $0.25 M_{\odot}$  steps. For the period, I chose a range of  $5 \rightarrow 30$  days, as a large amount of the periods in table 1 from [Fortin et al. \(2022\)](#) are in this range. It should be noted that those periods have been measured after a supernova has occurred in the system.

I kept the following parameters constant for all of my simulations -

- Simulation time - 20 Myr.
- Metallicity - 0.012.
- Eccentricity - 0.1.

I chose to run the simulations for 20 Myr as massive stars have very short lifetimes before going supernova, so there was no need to run them for longer. Following [Moe & Di Stefano \(2017\)](#) who state that short period binaries (of period  $P \leq 20$  days) typically have low eccentricities, I choose a low eccentricity of 0.1. Of course the distribution in reality certainly isn't a constant, this is perhaps something to explore in the future. I chose 0.012 as the metallicity as it is the solar metallicity. The potential ramifications of these assumptions will be discussed in more detail in section 6.2.2.

### 4.2.2 Selecting the Final Data

I needed to choose a consistent time to take the data for the parameters of the systems. By default, COSMIC outputs 4 pandas ([pandas development team \(2020\)](#) & [Wes McKinney \(2010\)](#)) dataframes - one containing parameters at key evolutionary steps (bpp), one at user specified steps (bcm), one containing the initial conditions (initC), and one containing the kicks and systemic/peculiar velocities (kick\_info). It is simple to get the correct system velocities from the kick\_info dataframe, however selecting a consistent point to sample the mass is more tricky. I achieved this by specifying conditions for the bcm array that output only the times where the system was an HMXB. I then chose the earliest time in the dataframe for which the system was an HMXB. A note is that some of the simulated systems



will never become HMXBs, instead merging or disrupting before they become one. This is not a problem - the bcm dataframe contained an extra line showing if the system had merged. Once the full simulation was complete, I could simply remove the merged systems before plotting. Disrupted systems can be removed in a similar fashion. In addition, since my data from *Gaia* and literature only contains NS HMXBs, I only want to plot systems in which the compact object is a neutron star. Therefore, I removed any systems that resulted in the formation of a black hole.

## 5 SIMULATION RESULTS

For each simulation, I have created a plot with the same axes as the one using data from *Gaia* (figure 2), plotting the peculiar/systemic velocity against the companion mass. For the simulations in which I varied the period and companion mass, I have created a grid of the initial companion mass and period, then coloured each point by the maximum survival velocity. Only simulations which produced a NS HMXB at the time when I recorded the mass are included on these plots.

### 5.1 Default Kick

Figures 3, 4, and 5 use the default kick mechanism from COSMIC.

#### 5.1.1 Companion and Progenitor Mass

Figure 3 shows a clear negative correlation between velocity and companion mass. This is in stark contrast to the actual data in figure 2. There is also a notable gap in the final companion mass around  $25 \rightarrow 27M_{\odot}$ , and a smaller one around  $30M_{\odot}$ . In section 5.5, I discuss what could cause this discontinuity.

#### 5.1.2 Companion and Period

Figure 4 shows that for low period and mass no systems survived the kick and produced a neutron star - there are no data points at the bottom left of the graph. For systems of low initial mass, only short periods in the range of  $\approx 7 \rightarrow 13$  days survived. High masses and low periods also did not survive. Interestingly as you move to the top left of the graph stars appear to stop surviving. It appears that closer to the top left of the graph, less systems survive. This behaviour is not present in other kick prescriptions for unknown reasons, figures 7, 10, and 13.

Again, the companion mass systemic velocity plot, 5 produces a correlation that doesn't agree with data. The velocities in this plot are much higher, up to  $200 \text{ km s}^{-1}$ . This isn't inconsistent with figure 3, as here the lowest mass is much lower,  $\approx 5M_{\odot}$  compared to  $\approx 22M_{\odot}$ . When comparing the plots over the same mass range, the velocities are broadly similar.

### 5.2 Kick A

Figures 6, 7, and 8 use kick prescription A, equation 2.

#### 5.2.1 Companion and Progenitor Mass

Figure 6 again has the incorrect correlation, and mass gap in a similar location as figure 3. It differs in 2 major ways. The velocities overall are much lower than for the default kick, and that more systems

Systemic Velocity Against Final Companion Mass  
Default Kick Prescription

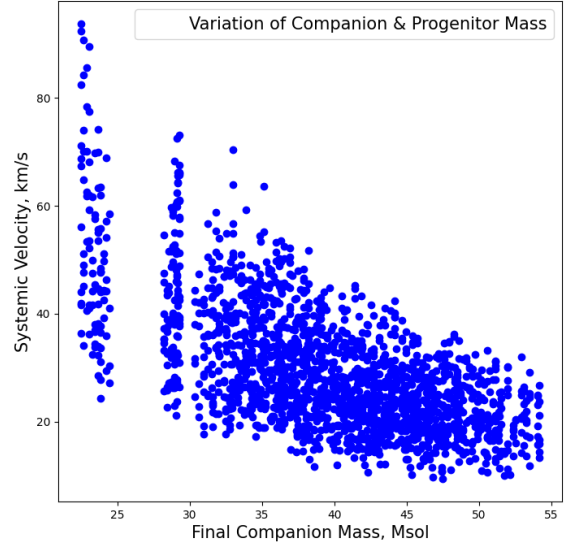


**Figure 3.** Peculiar/Systemic Velocity ( $\text{km s}^{-1}$ ) against Final Companion Mass ( $M_{\odot}$ ). This plot uses the default kick prescription from COSMIC and involved the variation of both the companion and progenitor star masses from  $20 \rightarrow 60M_{\odot}$  in steps of  $1M_{\odot}$ . Only systems which successfully became NS HMXBs are included.

Initial Period against Initial Companion Mass,  
Coloured by Max Surviving Systemic Velocity (km/s)  
Default Kick Prescription

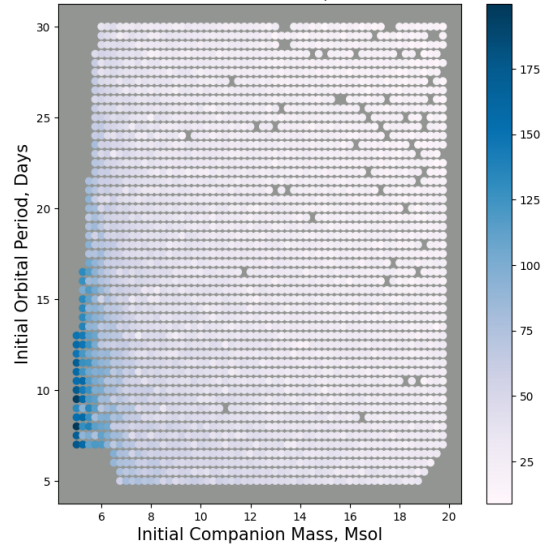


**Figure 4.** Initial Orbital Period (days) against initial Companion Mass ( $M_{\odot}$ ), coloured by the maximum velocity in which a NS HMXB was produced. This plot uses the default kick prescription from COSMIC and involved the variation of the orbital period from  $5 \rightarrow 30$  days in steps of  $0.5$  days, and the companion star mass from  $5 \rightarrow 19.75M_{\odot}$  in steps of  $0.25M_{\odot}$ . The progenitor star mass was kept at  $20M_{\odot}$ .

Systemic Velocity Against Final Companion Mass  
Default Kick Prescription

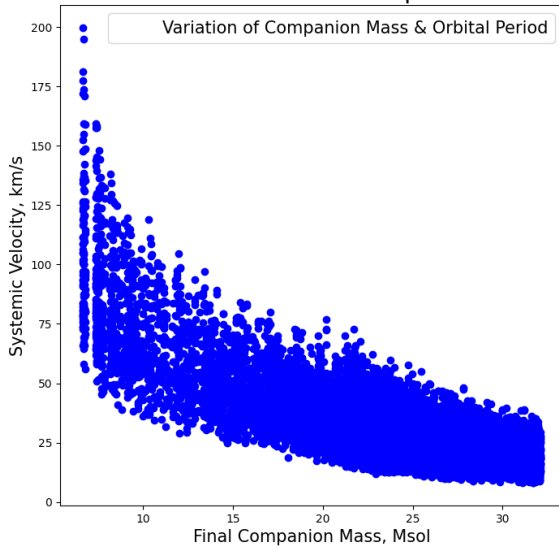


**Figure 5.** Peculiar Velocity ( $\text{kms}^{-1}$ ) against Final Companion Mass ( $M_{\odot}$ ). This plot uses the default kick prescription from COSMIC and involved the variation of the orbital period from  $5 \rightarrow 30$  days in steps of 0.5 days, and the companion star mass from  $5 \rightarrow 19.75M_{\odot}$  in steps of  $0.25M_{\odot}$ . The progenitor star mass was kept at  $20M_{\odot}$ .

survived the supernova which is clearly seen by the amount of points on the graph.

### 5.2.2 Companion and Period

Figure 7 is broadly similar to the default kick figure. The only major differences are again the lower overall velocity (as shown clearly by the colour bar on the side) and the fact that there are no missing systems as you move to the top right. In addition, the distribution of velocities appears to be a lot more uniform near the high end, compared to figure 4. This is likely due to the fact that a larger amount of systems for prescription A survived the supernova, smoothing out the velocity distribution.

Figure 8 shows similar differences as figure 6 does - more surviving systems, and lower velocities overall. There is some interesting behaviour at masses  $\approx 15 \rightarrow 20M_{\odot}$  - some spikes in the maximum surviving velocity appear. What causes this is unclear.

## 5.3 Kick B

Figures 9, 10, and 11 use kick prescription B, equation 3.

### 5.3.1 Companion and Progenitor Mass

Figure 9 shows the same behaviour as the previous 2 kick prescriptions. It appears to be a middle ground of the two - the maximum surviving velocities are between those of figures 3 and 6. The same can be said about the amount of surviving systems. One key difference however is that there appears to be a few systems between the

Systemic Velocity Against Final Companion Mass  
Kick Prescription A

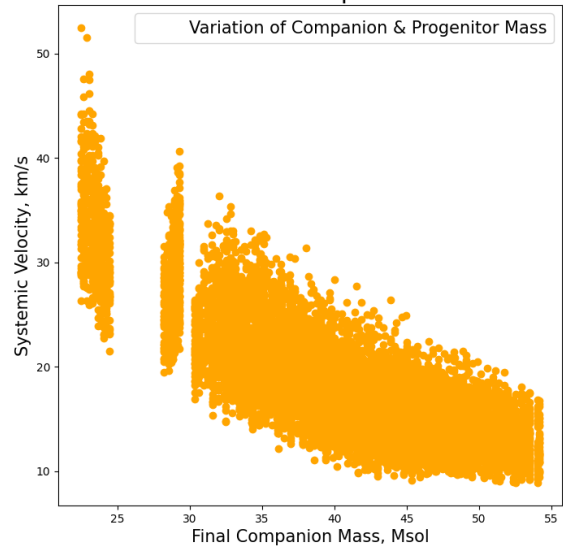


**Figure 6.** Peculiar/Systemic Velocity ( $\text{kms}^{-1}$ ) against Final Companion Mass ( $M_{\odot}$ ). This plot uses kick prescription A and involved the variation of both the companion and progenitor star masses from  $20 \rightarrow 60M_{\odot}$  in steps of  $1M_{\odot}$ . Only systems which successfully became NS HMXBs are included.

Initial Period against Initial Companion Mass,  
Coloured by Max Surviving Systemic Velocity ( $\text{km/s}$ )  
Kick Prescription A

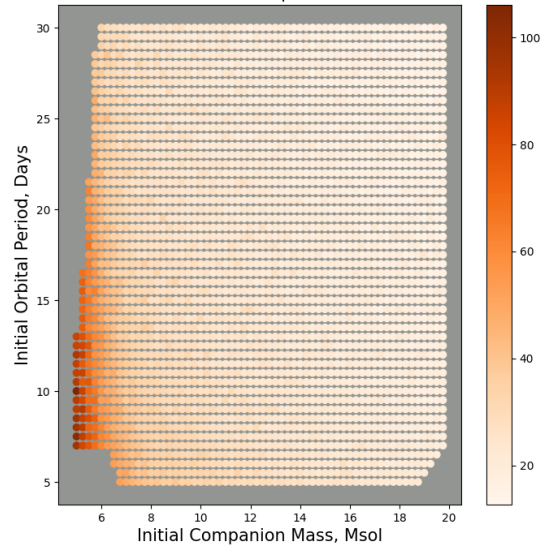


**Figure 7.** Initial Orbital Period (days) against initial Companion Mass ( $M_{\odot}$ ), coloured by the maximum velocity in which a NS HMXB was produced. This plot uses kick prescription A and involved the variation of the orbital period from  $5 \rightarrow 30$  days in steps of 0.5 days, and the companion star mass from  $5 \rightarrow 19.75M_{\odot}$  in steps of  $0.25M_{\odot}$ . The progenitor star mass was kept at  $20M_{\odot}$ .

Systemic Velocity Against Final Companion Mass  
Kick Prescription A

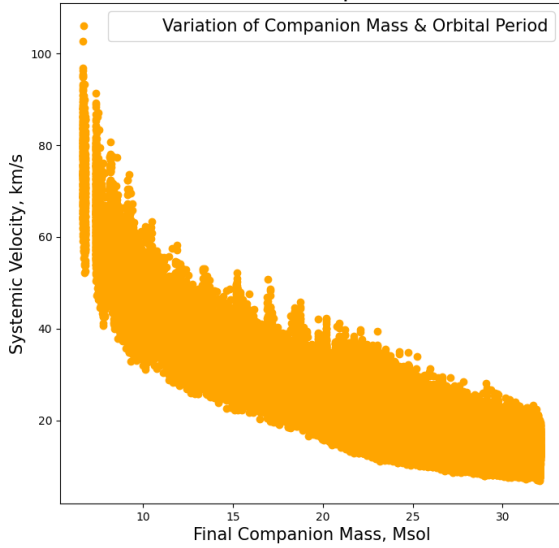


**Figure 8.** Peculiar Velocity ( $\text{kms}^{-1}$ ) against Final Companion Mass ( $M_{\odot}$ ). This plot uses kick prescription A and involved the variation of the orbital period from  $5 \rightarrow 30$  days in steps of 0.5 days, and the companion star mass from  $5 \rightarrow 19.75 M_{\odot}$  in steps of  $0.25 M_{\odot}$ . The progenitor star mass was kept at  $20 M_{\odot}$ .

mass range of  $\approx 27 \rightarrow 37$  which have abnormally high velocities. The behaviour does not occur for kick prescription A however it does for the default prescription, albeit to a lesser degree.

### 5.3.2 Companion and Period

There is nothing interesting to be said about figures 10 and 11. They appear to be a middle ground between the other two kick prescriptions, as mentioned in section 5.3.1.

## 5.4 No Asymmetric Kicks

Figures 12, 13, and 14 are all using no asymmetric kicks.

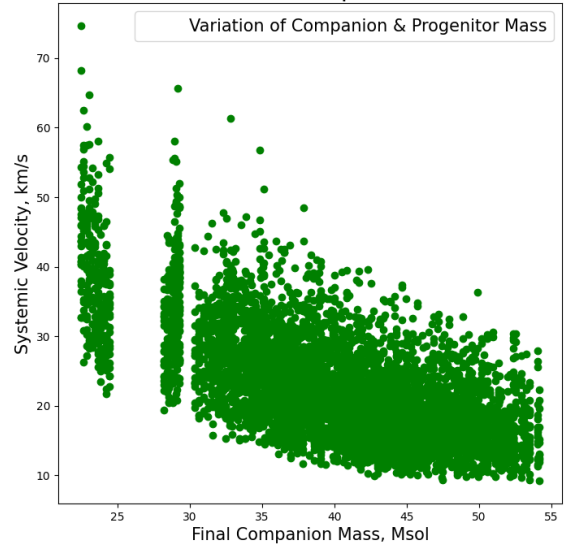
### 5.4.1 Companion and Progenitor Mass

Figure 12 looks vastly different to the figures which involve kicks. The overall velocities are far lower (as expected, I had removed the main source of the high velocities) and there are far fewer data points. This is easily explained - the generation of the asymmetric kicks is the only source of randomness in the simulations that I ran. Once this source of randomness is removed, all of the systems in a given starting state evolve in exactly the same fashion. The higher mass systems have lower peculiar velocities - this is known information. We can even derive the relation between the kick velocity and mass loss for symmetric kicks, see section 6 of [Blaauw \(1961\)](#).

### 5.4.2 Companion and Period

The same can be said from section 5.4.1 for figure 14. A combination of mass and period results in the same evolutionary state every time.

Systemic Velocity Against Final Companion Mass  
Kick Prescription B



**Figure 9.** Peculiar/Systemic Velocity ( $\text{kms}^{-1}$ ) against Final Companion Mass ( $M_{\odot}$ ). This plot uses kick prescription B and involved the variation of both the companion and progenitor star masses from  $20 \rightarrow 60 M_{\odot}$  in steps of  $1 M_{\odot}$ . Only systems which successfully became NS HMXBs are included.

Initial Period against Initial Companion Mass,  
Coloured by Max Surviving Systemic Velocity ( $\text{km/s}$ )  
Kick Prescription B

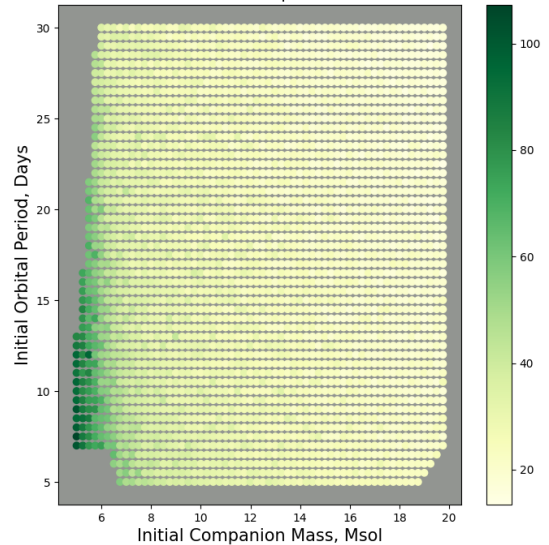


**Figure 10.** Initial Orbital Period (days) against initial Companion Mass ( $M_{\odot}$ ), coloured by the maximum velocity in which a NS HMXB was produced. This plot uses kick prescription B and involved the variation of the orbital period from  $5 \rightarrow 30$  days in steps of 0.5 days, and the companion star mass from  $5 \rightarrow 19.75 M_{\odot}$  in steps of  $0.25 M_{\odot}$ . The progenitor star mass was kept at  $20 M_{\odot}$ .



### Systemic Velocity Against Final Companion Mass Kick Prescription B

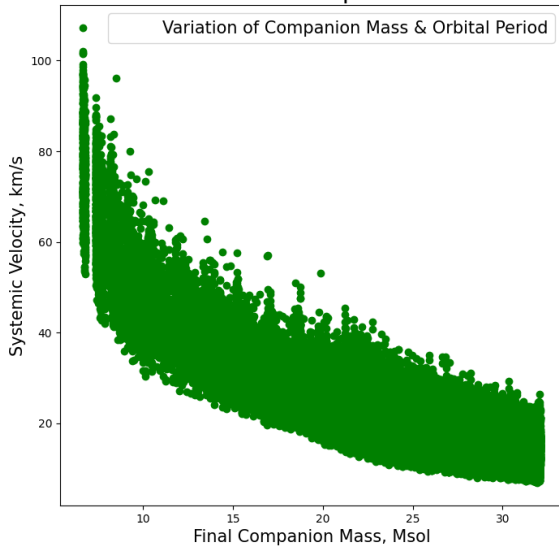


**Figure 11.** Peculiar Velocity ( $\text{kms}^{-1}$ ) against Final Companion Mass ( $M_{\odot}$ ). This plot uses kick prescription B and involved the variation of the orbital period from  $5 \rightarrow 30$  days in steps of 0.5 days, and the companion star mass from  $5 \rightarrow 19.75M_{\odot}$  in steps of  $0.25M_{\odot}$ . The progenitor star mass was kept at  $20M_{\odot}$ .

### Systemic Velocity Against Final Companion Mass No Asymmetric Kicks

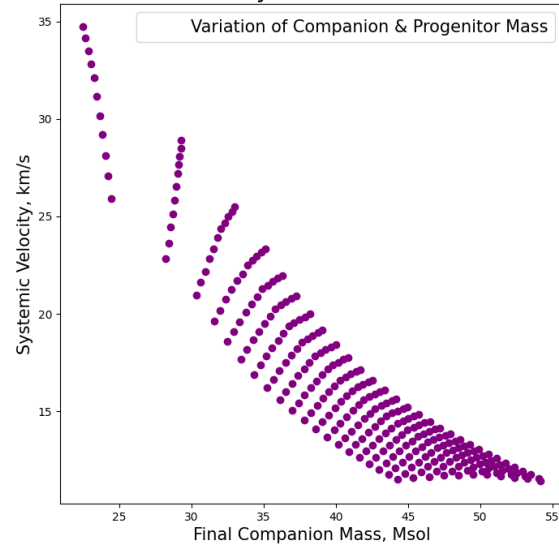


**Figure 12.** Peculiar/Systemic Velocity ( $\text{kms}^{-1}$ ) against Final Companion Mass ( $M_{\odot}$ ). This plot disabled asymmetric kicks and involved the variation of both the companion and progenitor star masses from  $20 \rightarrow 60M_{\odot}$  in steps of  $1M_{\odot}$ . Only systems which successfully became NS HMXBs are included.

### Initial Period against Initial Companion Mass, Coloured by Max Surviving Systemic Velocity (km/s) No Asymmetric Kicks

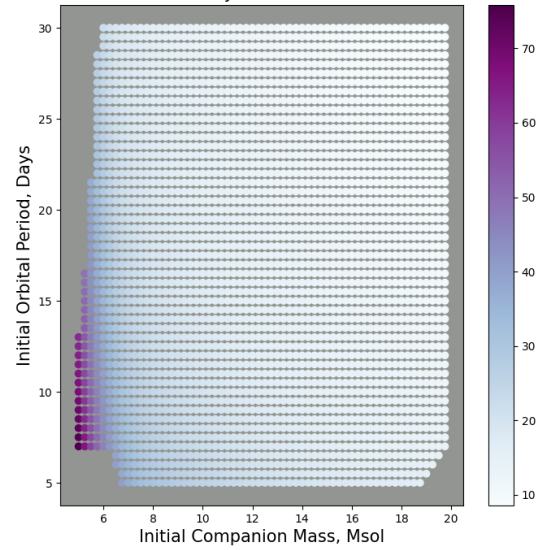


**Figure 13.** Initial Orbital Period (days) against initial Companion Mass ( $M_{\odot}$ ), coloured by the maximum velocity in which a NS HMXB was produced. This plot disabled asymmetric kicks and involved the variation of the orbital period from  $5 \rightarrow 30$  days in steps of 0.5 days, and the companion star mass from  $5 \rightarrow 19.75M_{\odot}$  in steps of  $0.25M_{\odot}$ . The progenitor star mass was kept at  $20M_{\odot}$ .

The velocity decreases with mass as well. The plot also appears more dense and this is simply because there are many more total simulated systems here - over 3 times as many. The grid of masses and periods in figure 13 is completely smooth (as expected due to the lack of randomness, and again has corners where no systems survived).

## 5.5 Mass Gap

### 5.5.1 Investigating The Mass Gap

The mass gap is a consistent artefact appearing for every plot in which I varied the mass of both stars. For all of the following tests I used the default kick prescription, as the others seem to just scale the final velocities.

Firstly, I will include all the systems that resulted in Black holes, shown in figure 15. This does not solve the problem. While it fills most of the smaller gap at just below  $30M_{\odot}$ , it creates a new gap between  $\approx 13 \rightarrow 20M_{\odot}$ . The next test is to include disrupted systems. It is no use plotting mergers as they are considered as mass-less remnants by COSMIC and thus have 0 mass. Figure 16 includes disrupted systems. It now shows systems of much higher velocity, all of which are disrupted binaries. The mass gap is still present. Next up is to create a grid of the parameter space to see what happened to the systems of different mass Pairings.

### 5.5.2 Survived

In figure 17 which shows the survival percentage, one can see that systems with low masses for both stars generally didn't survive the supernova. Very few systems survived for high progenitor mass and

Systemic Velocity Against Final Companion Mass  
No Asymmetric Kicks

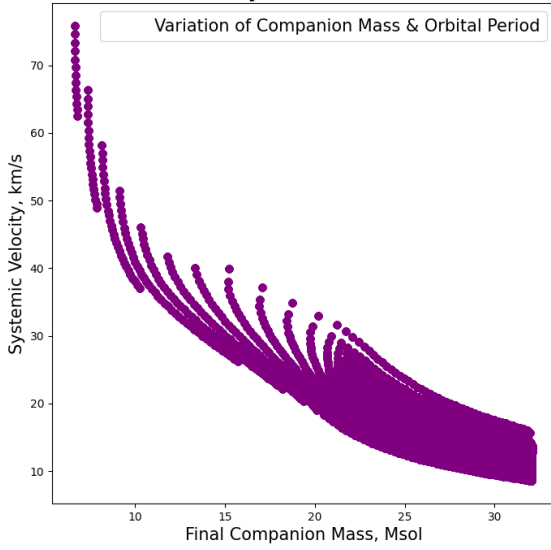


**Figure 14.** Peculiar Velocity ( $\text{kms}^{-1}$ ) against Final Companion Mass ( $M_{\odot}$ ). This plot disabled asymmetric kicks and involved the variation of the orbital period from 5  $\rightarrow$  30 days in steps of 0.5 days, and the companion star mass from 5  $\rightarrow$   $19.75M_{\odot}$  in steps of  $0.25M_{\odot}$ . The progenitor star mass was kept at  $20M_{\odot}$ .

Systemic Velocity Against Final Companion Mass  
Default Kick Prescription

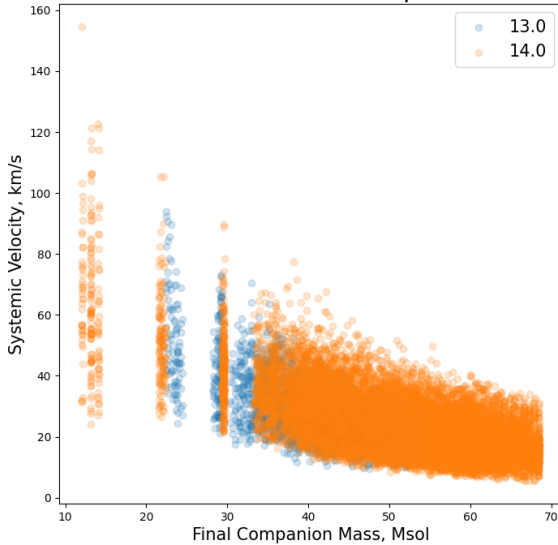


**Figure 15.** Peculiar/Systemic Velocity ( $\text{kms}^{-1}$ ) against Final Companion Mass ( $M_{\odot}$ ). This plot uses the default kick prescription from COSMIC and involved the variation of both the companion and progenitor star masses from 20  $\rightarrow$   $60M_{\odot}$  in steps of  $1M_{\odot}$ . Orange points labelled as 14 signify BH HMXBs, and blue points labelled as 13 signify NS HMXBs.

Systemic Velocity Against Final Companion Mass  
Default Kick Prescription

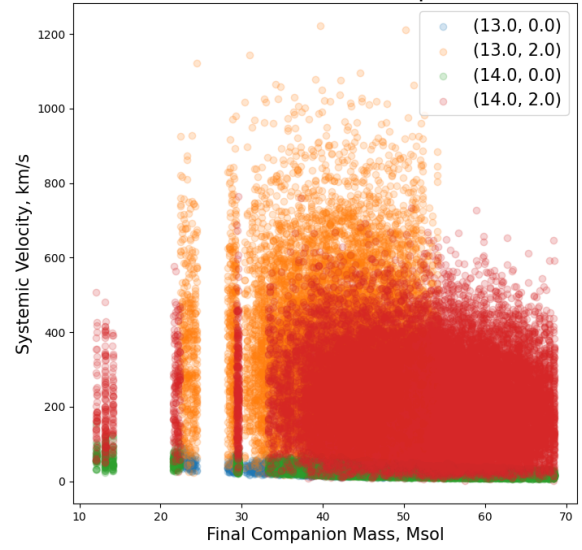


**Figure 16.** Peculiar/Systemic Velocity ( $\text{kms}^{-1}$ ) against Final Companion Mass ( $M_{\odot}$ ). This plot uses the default kick prescription from COSMIC and involved the variation of both the companion and progenitor star masses from 20  $\rightarrow$   $60M_{\odot}$  in steps of  $1M_{\odot}$ . Points with a first label of 13 or 14 are simulations which resulted in a NS or BH respectively. Points with a secondary label of 0 or 2 correspond to systems that survived or were disrupted respectively.

low companion mass as can be seen in the top left corner of the figure.

### 5.5.3 Disrupted

Figure 18 shows the percentage of systems which were disrupted during evolution. Disruption was most likely to occur for systems of low progenitor and companion mass, and is quite common overall. The exception to this is systems of high progenitor mass and low companion.

### 5.5.4 Merged

Figure 19 shows the percentage of systems which merged. Overall, very few systems merged during evolution, with one major exception. Systems of high initial progenitor mass and low initial companion mass were highly likely to merge. After looking directly at the data files, all dark spots in the top left corner had 100% of systems merge.

### 5.5.5 Binary Evolution Plots

Figures 20, and 21 plot initial against final companion mass. Figure 20 is coloured by initial companion mass and contains only a few initial masses. I have excluded merged systems from these plots, as they would just congregate around  $0M_{\odot}$  on the x axis. Figure 21 shows a huge range of masses that are simply never produced in my evolution.

Figures 23, 24, 25, 26, 27, 28, 29, 30, 31, 32 located in section 8 for ease of access, trace the evolution of various mass pairings over

Initial Progenitor against Initial Companion Mass  
Coloured by Percentage Survived  
Default Kick Prescription

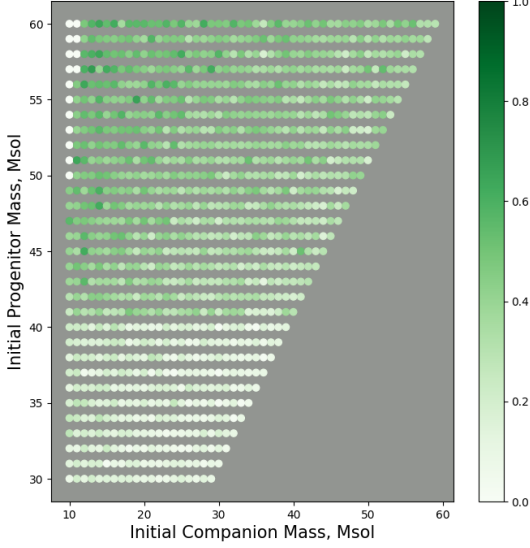


**Figure 17.** Initial Progenitor against Initial Companion Mass ( $M_{\odot}$ ). This plot uses the default kick prescription from COSMIC and involved the variation of both the companion and progenitor star masses from  $20 \rightarrow 60 M_{\odot}$  in steps of  $1 M_{\odot}$ . Points are coloured by the percentage of simulations of a given initial mass pairing that survived the supernova.

Initial Progenitor against Initial Companion Mass  
Coloured by Percentage Merged  
Default Kick Prescription

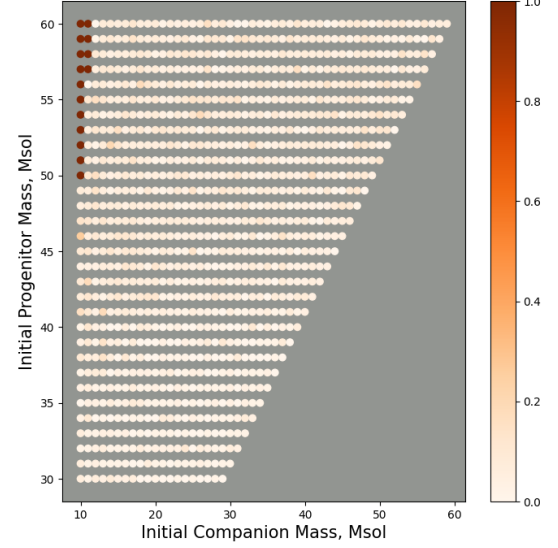


**Figure 19.** Initial Progenitor against Initial Companion Mass ( $M_{\odot}$ ). This plot uses the default kick prescription from COSMIC and involved the variation of both the companion and progenitor star masses from  $20 \rightarrow 60 M_{\odot}$  in steps of  $1 M_{\odot}$ . Points are coloured by the percentage of simulations of a given initial mass pairing that merged during evolution.

Initial Progenitor against Initial Companion Mass  
Coloured by Percentage Disrupted  
Default Kick Prescription

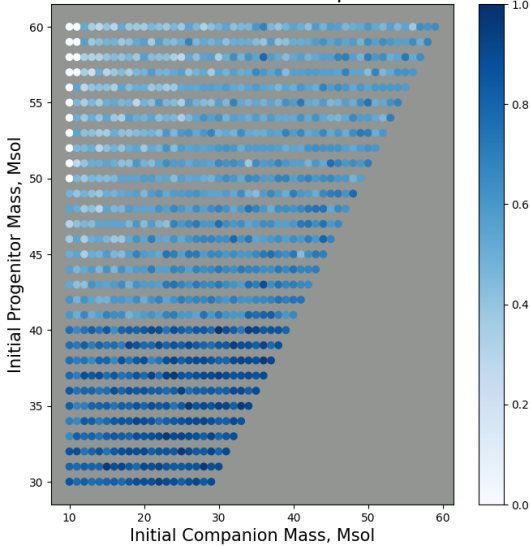


**Figure 18.** Initial Progenitor against Initial Companion Mass ( $M_{\odot}$ ). This plot uses the default kick prescription from COSMIC and involved the variation of both the companion and progenitor star masses from  $20 \rightarrow 60 M_{\odot}$  in steps of  $1 M_{\odot}$ . Points are coloured by the percentage of simulations of a given initial mass pairing that disrupted after the supernova.

Final Companion Mass Against Initial Companion Mass  
Coloured by Initial Progenitor Mass  
Default Kick Prescription

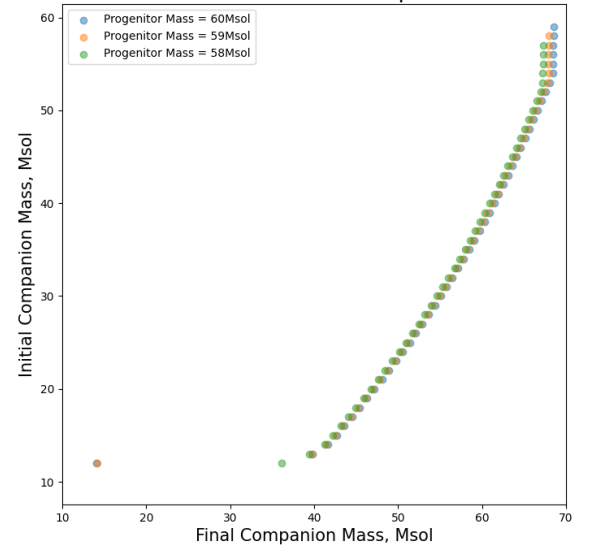


**Figure 20.** Initial Companion against Final Companion Mass ( $M_{\odot}$ ). This plot uses the default kick prescription from COSMIC and involved the variation of both the companion and progenitor star masses from  $20 \rightarrow 60 M_{\odot}$  in steps of  $1 M_{\odot}$ . Points are coloured by the Initial Progenitor Mass. This plot only contains progenitor masses of  $58 \rightarrow 60 M_{\odot}$ .

Final Companion Mass Against Initial Companion Mass  
Default Kick Prescription

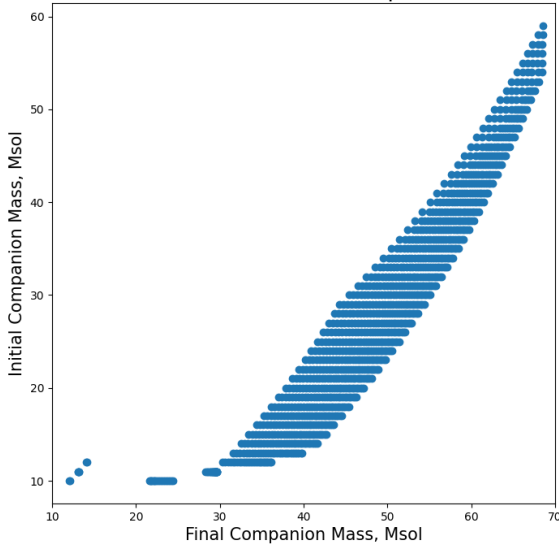


**Figure 21.** Initial Companion against Final Companion Mass ( $M_{\odot}$ ). This plot uses the default kick prescription from COSMIC and involved the variation of both the companion and progenitor star masses from  $20 \rightarrow 60M_{\odot}$  in steps of  $1M_{\odot}$ .

time. In section 6.3, I will analyse how these plots explain the gap.

### 5.6 Similar Mass Generation

Motivated by the reasons outlined in section 4.2.1, I performed a simulation with a more limited parameter space to see if any major changes would occur. For this test I am not taking into account whether this limitation is actually physical or not, as I am only interested in learning whether such a limitation could cause a major change in the result. For the limitation, I chose to only generate masses of stars within  $5M_{\odot}$  of each other. I used the default kick prescription and a mass range of  $10 \rightarrow 60M_{\odot}$  for the progenitor star in steps of  $1M_{\odot}$ . I used a step of  $0.25M_{\odot}$  for the small  $5M_{\odot}$  range below the progenitor mass for the companion. The resulting graph can be seen in figure 22. The shape of the curve is entirely different, and even appears to have a slight positive slope on top. However, the peculiar velocities of these systems are far lower than what we observe in figure 2.

### 5.7 Limitations and Comments

This project had one main limitation, that of time. Running the simulations took a long time - each run of a period-companion simulation took approximately 3 hours, and the dual mass simulations took about 1 hour. This limitation became worse due to the fact I had very limited total computing time. For future research an obvious thing to do would be to explore more of the parameter space - vary all of both masses, periods, and eccentricities. I could also change a variety of other flags within COSMIC concerning more complex parts of binary evolution, including winds, common envelope evolution, mass transfer etc. I could also change more kick flags to modify how they

Systemic Velocity Against Final Companion Mass  
Default Kick Prescription

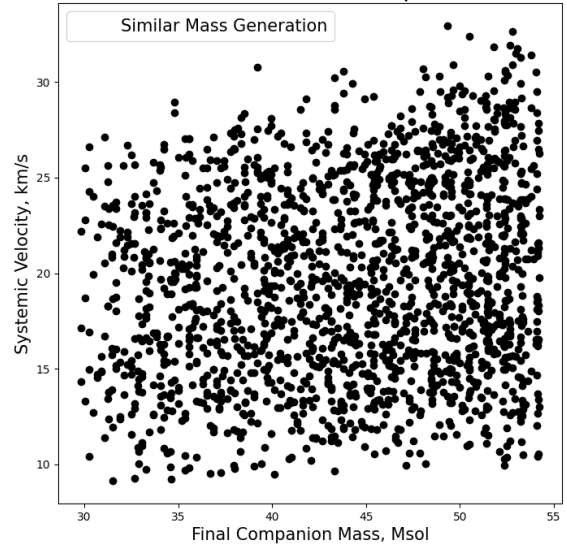


**Figure 22.** Peculiar/Systemic Velocity ( $\text{km s}^{-1}$ ) against Final Companion Mass ( $M_{\odot}$ ). This plot uses the default kick prescription from COSMIC. Here, the progenitor mass was varied from  $10 \rightarrow 60M_{\odot}$  in steps of  $1M_{\odot}$ . The companion star was restricted to being within  $5M_{\odot}$  below the progenitor mass, and the mass was generated at steps of  $0.25M_{\odot}$  within this interval. Only systems which successfully became NS HMXBs are included.

occur. My simulations assume that the direction of the asymmetric kicks are isotropic in their distribution - however there is evidence to suggest that kicks may be preferentially directed along the spin axis of the newly formed compact object - Wang et al. (2006), Ng & Romani (2007), and Kaplan et al. (2008). This would be something to explore further.

## 6 DISCUSSION

### 6.1 Peculiar Velocities and Asymmetric Kicks

Figure 2 clearly shows that binary systems with a larger companion mass have larger peculiar velocities. One might question what could possibly cause a binary system to move in the first place, and if we can attribute any of these velocities to causes other than supernova.

A first reason could be that the systems were simply formed at such velocities. Young stars are known to form at velocities up to  $30\text{km s}^{-1}$  as per Baba et al. (2009), so perhaps the HMXBs below this velocity were formed that way. I believe this to be unlikely as we know one of the stars in the system must have gone supernova, and so there must have been a change in peculiar velocity at some point during evolution. Even excluding asymmetric kicks, from the simulations in section 5.4, we know that due to momentum conservation a star going supernova must impart a kick due to mass loss. So while the total peculiar velocity may not be entirely due to a supernova, a component of it must be. If one were to remove these low velocity systems for the sake of argument, there is clearly no correlation between companion mass and peculiar velocity. However if we were to indeed see this result, we just have more questions - why do we not see HMXBs with low peculiar velocities?

An alternative reason could be the system approaching another



stellar object (be it a heavy black hole, a more massive star, or even another binary system) and getting a boost in velocity. This is unlikely to occur for these systems however, as they live in the disc of the Milky Way where encounters are scarce. If an encounter did occur in any case, they tend to cause disruption, collisions, large changes in eccentricity, and other effects rather than a velocity boost (Hills (1975), Kaib & Raymond (2014), Hamers & Samsing (2019)).

A velocity kick at birth avoids these problems - while we don't understand the mechanism by which they occur (although there are many theories, see Lai (2001) for a summary) they can impart kicks independent of how the stars were born, or from stellar encounters. The problem is that the mechanism behind kicks provides no explanation for the data. After all, figure 2 contains no information about the progenitor star or specifics about its evolutionary history. We only know that a neutron star was produced, and that the higher the companion mass to this star, the higher the peculiar velocity generally is. This leads me to believe that this result is more a question of binary evolution than of supernova kicks.

## 6.2 Simulation Results

It is clear that the simulations do not produce what we see in reality. The observed correlation is nowhere to be seen, and the velocities produced by the simulations are not accurate to the velocities we observe. Here I will discuss two potential causes for this discrepancy. These are either that the simulated kicks/evolution of the binary systems is not accurate to reality, or the assumptions put into the generation of my systems aren't realistic.

### 6.2.1 Kick Generation

Kick generation in COSMIC is rather simple, as the kicks are either simply pulled from one distribution and applied isotropically (for kick prescriptions A and B), or are sampled from multiple distributions dependant on the type of supernova as for the default prescription. The distributions are calculated from fitting to data, in particular the  $\sigma = 265 \text{ km s}^{-1}$  dispersion used for the standard kick was calculated by Hobbs et al. (2005). This was calculated via the usage of single stars, so it is perhaps not surprising that this distribution does not work when considering binaries.

COSMIC does give other parameters for kick generation, a particularly interesting one being restricting the direction of the kicks to near the spin axis of the progenitor star. There is observational evidence to support this, Wang et al. (2006), Ng & Romani (2007), and Kaplan et al. (2008), where the proper motions of pulsars were found to be correlated with their spin axis. Depending on whether or not the spin and orbit of the binary tends to be aligned or not in reality could determine how much an effect this constraint has. While one might expect for spin and orbit to often be aligned due to tidal forces, this might not be the case (Justesen & Albrecht (2020), Albrecht et al. (2009)) and there can be spin-orbit misalignment. If one were to make a naive assumption that the spin and orbit are entirely independent of each other constraining kicks to the spin axis would be no different than generating them isotropically. If spins happened to be more likely aligned with the orbit and kicks were generated preferentially in this direction, one would have less kicks directed directly at or away from the companion star. This could have ramifications on how often binaries disrupt, merge or survive the supernova.

### 6.2.2 System Generation

As mentioned in section 4.2.1, my assumptions when generating the systems could have a large impact. A rather extreme example is shown in 22, which has a completely different correlation compared to the rest of my simulations. While it does not have any resemblance to reality (the velocities produced are far too low for a given companion mass, and there is little to no correlation) it does show that changing how the systems are formed and exist could give vastly different results. Assuming similarly generated masses might seem like an arbitrary test, however it is not unfounded. We have compiled mass ratios for many binary stars, and found the distribution to not be uniform. For example Valtonen (1997) found that for single-lined spectroscopic binaries with B type primary stars the mass ratio distribution goes as  $\psi_q(q) \propto q^{-2}$  for  $q > q_0$ , with  $q_0 = 0.3$ , and the distribution is flat for  $q < q_0$ , with  $q$  representing the mass ratio,  $q = \frac{M_{\text{secondary}}}{M_{\text{primary}}}$ . They quote that the value of  $q_0$  changes to 0.5 for K-Type primaries. The changing of this critical value is unlikely to change my simulations as I always generated primary stars well into the O class. For double-lined spectroscopic binaries Valtonen (1997) say that the distribution shape is almost entirely dominated by selection effects. When taking a sub-sample constricted by magnitude (as they are less affected by the selection effects), a similar relation was retrieved over a different interval of  $q$ .

We observe binary systems of immensely different periods, from short periods of order  $\approx 1$  day to long periods of order  $\approx 10^{10}$  days, as specified in Kroupa & Burkert (2001). It is unrealistic to explore this parameter space in its entirety. An easy way to limit this space is to look for a bias in periods for HMXBs. Table 2 in Sidoli & Paizis (2018) and table 1 in Fortin et al. (2022) show parameters for many HMXBs. Periods seem to mostly be of the order of 10 days, with some reaching to  $10^{-1}$  or  $10^2$ , but not much longer or shorter than those. I therefore believe that my range of chosen periods is appropriate. Figure 4 in Moe & Di Stefano (2017) shows a plot of the mass ratios for a range of binaries against their orbital periods. For my range of periods ( $5 \rightarrow 30$  days,  $\approx 0.7 \rightarrow 1.4$  days in log space), there is a noticeable lack of systems of log period  $1 \rightarrow 1.5$  with mass ratios of  $\approx 0.4$ , which would be included in my parameter space. It simply could be that we are yet to observe systems of these parameters (as we have limited data on these binary systems).

Looking at these possible relations between mass ratio, period, and eccentricity, and figure 22 it is therefore not unrealistic that implementing a more realistic exploration of the parameter space could result in vastly different results, and therefore a different outcome of systemic velocity and companion mass.

## 6.3 Mass Gap

In all of the simulations where kicks were enabled, there is a curious gap in the final companion masses produced, which can be seen in figures 3, 6, and 9. When investigating I decided to include the systems which resulted in BHs in addition to the neutron stars and this created an even larger gap. Figure 15 shows this. I produced a number of graphs shown in section 5.5, to figure out the cause. From figures 23, 24, 26, 28, and 30 you can see that if the binary system undergoes a longer period of Core Helium Burning (CHeB, signified by neon green), the system merges. If there is a short period of CHeB, as in figures 29 and 32, then the companion star will receive a large amount mass from the progenitor and the system survives. Without this brief period of CHeB, the companion star gets very little mass from the progenitor, shown in figures 25, 27, and 31. For reasons unknown, some pairs of masses simply do not transfer mass between



the stars and others simply merge instead. The systems which transfer only a little mass can be seen at around  $12M_{\odot}$  in figure 21, and the systems which survive the explosion and transfer significant mass can be seen all grouped together at  $\approx 22M_{\odot}$ . I believe that if mass transfer had occurred similarly to the rest of the systems, the small group of systems around  $\approx 12M_{\odot}$  would move to the right, and thus remove the gap.

As mentioned in section 5.4, the only source of randomness in these simulations is the generation of the asymmetric kick. This results in the same starting masses resulting in the same final masses at the time of measurement for all simulations. Since my mass generation was quite coarse, I would expect some gaps to naturally arise as a result. I believe this is the cause of the mass gaps at around  $\approx 25M_{\odot}$  and  $\approx 30M_{\odot}$  in figure 15. This can be seen explicitly in figure 21, where there is a larger gap around  $25M_{\odot}$ , and a place where the final masses just barely overlap at  $30M_{\odot}$ .

#### 6.4 Final Comments

The question becomes is if the potential changes discussed were to be implemented, would we obtain the observed result? I think it unlikely that basic changes to the kick prescription (ones that involve simple scaling factors) or an understanding of the explicit underlying physics of kicks (at least, for single stars) would help. After all, there is nothing particularly interesting about the result found from figure 2 without the knowledge that these data points are in HMXBs. The relation shown in the plot is more a question of binary evolution - how the stars in the systems are born, interact, and evolve. There are many facets of binary evolution, of which some we understand very little of. One such example is common envelope evolution, [Ivanova et al. \(2013\)](#). Once the progenitor goes supernova, that's it for that part of the physics - what occurs before and after is purely binary evolution. Considering this, perhaps it is not surprising that the mass gap discussed in section 6.3 is unrelated to kicks - the systems that merged all did so before the supernova even occurred.

A method in which binary evolution may affect the kick velocities is explored by [van den Heuvel et al. \(2000\)](#). They find that supergiant systems systematically have narrower orbits pre-supernova than smaller Be systems, due to them having higher fractional helium core mass. They also state that more massive systems eject much more mass. For these reasons, they expect that higher mass systems might suffer more massive kicks. This would explain the relation in figure 2. COSMIC does not implement this helium core interaction, so perhaps including it may allow it to produce the observed result.

#### 6.5 Future Research

For the future, a first thing to do is observe more HMXB systems and calculate their peculiar velocities. The more systems there are in the data set the more sure we can be that the observed correlation is significant. If it is indeed so, then we should look at our models of binary evolution. There are still many parts we do not understand fully, and perhaps if we were to implement a more accurate treatment then we might recreate what we see. Even if we don't understand the internal physics of how a kick might occur, we do know how to accurately generate the velocities they can impart on occurrence for single stars. Perhaps this treatment is inaccurate for binaries, as explored by [Fortin et al. \(2022\)](#) - who find the peculiar velocities for NS HMXBs are better described by a gamma function. For this reason I believe that a more thorough understanding of the internal physics of kicks for single stars won't help us in understanding this

peculiar result - we should look more into the epithets of binary evolution for answers.

## 7 CONCLUSIONS

(i) In this paper, I first calculated peculiar velocities for a variety of neutron star high-mass x-ray binary systems so that we may test our computational models of binary evolution. From the *Gaia* database, I collected 3D positional data (parallax, right ascension and declination) along with 2D velocities in the plane of the sky (proper motions). The final dimension of velocity was collected from a literature search. From the gathered data I calculated peculiar velocities for 16 systems, and plotted it against the companion mass. This results in a moderate positive correlation with a Pearson's R of 0.504, which is accepted at the 5% confidence interval.

(ii) I then moved to using the COSMIC binary synthesis suite in order to recreate this graph. I performed two types of simulations - one where the masses of both stars were changed, and the other keeping the progenitor mass constant whilst changing the companion mass and orbital period. For each simulation, I changed the prescription used for the asymmetric kicks as a result of one star going supernova. For all of the kick prescriptions I tested, none were able to replicate the result for peculiar velocities and companion masses given by data.

(iii) In the plots resulting from the mass varying simulations, a gap in the masses produced by the simulations emerged. When re-including systems that resulted in black hole HMXBs, a second, larger gap appeared. This larger gap was due to systems with a very high progenitor star mass ( $\approx 60M_{\odot}$ ) and low companion mass ( $\approx 10M_{\odot}$ ) either -

- Merging due to an extended period of core helium burning from the progenitor before supernova
- The companion star gaining a lot of mass from the progenitor due to a short period of core helium burning and ending up at a mass of  $\approx 22M_{\odot}$
- No core helium burning occurring and relatively little mass being transferred, with the companion masses being  $\approx 10M_{\odot}$

This created a large mass gap between  $\approx 10M_{\odot}$  and  $\approx 22M_{\odot}$ . The smaller mass gap visible on the plot only including NS HMXBs was due to my coarse generation of masses, necessitated by time limitations.

(iv) I then inquire into potential problems with my simulation methodology by testing if changing the distribution of masses generated could have any large effects of the shape of the resulting graph. For argument, I chose to only allow similar masses of companion and progenitor - this did indeed cause a massive change, making the relation between peculiar velocity and companion mass almost flat.

(v) Finally, I discuss what this means for our models. From data collated in previous research on single pulsars, [Hobbs et al. \(2005\)](#), we know how to generate accurate kick velocities for single stars. Understanding how these kick velocities occur will not change the resulting distribution. [Fortin et al. \(2022\)](#) find that kicks for these NS HMXBs are better described by a gamma function. Therefore I believe that the result of increasing peculiar velocity with companion mass is more of a question of binary evolution - why do kicks in binaries impart such different velocities to those applied to single stars? A possible evolutionary step to implement is discussed by [van den Heuvel et al. \(2000\)](#) involving large helium cores causing closer orbits in binaries for heavier systems. This results in heavier systems gaining higher peculiar velocities, and so could fix the problem.

## 8 EVOLUTION PLOTS

This section contains the plots of binary evolution used in sections 5.5.5 and 6.3 for ease of access and reading. The colour bars at the top of the plots denote the evolutionary stage of each star in the binary, with the top one being for the progenitor star and bottom the companion star. The plots below show how various quantities for the stars change over time, and are lined up with the evolutionary stage shown above them. The orange line denotes the companion star, the blue the progenitor. It is easy to see when a merger occurs - the evolutionary stage becomes "no remnant" and the mass drops to 0.

## ACKNOWLEDGEMENTS

This work has made use of data from the European Space Agency (ESA) mission *Gaia* (<https://www.cosmos.esa.int/gaia>), processed by the *Gaia* Data Processing and Analysis Consortium (DPAC, <https://www.cosmos.esa.int/web/gaia/dpac/consortium>). Funding for the DPAC has been provided by national institutions, in particular the institutions participating in the *Gaia* Multilateral Agreement.

This research has made use of the SIMBAD database, operated at CDS, Strasbourg, France.

Software: Python (<https://www.python.org/>), Numpy Harris et al. (2020), pandas pandas development team (2020) & Wes McK-inney (2010), COSMIC: <sup>1</sup> Breivik et al. (2020b)

This work made use of Astropy:<sup>2</sup> a community-developed core Python package and an ecosystem of tools and resources for astronomy Astropy Collaboration et al. (2013), Astropy Collaboration et al. (2018), Astropy Collaboration et al. (2022).

This work made use of the Astrophysics Data System (ADS) - <https://ui.adsabs.harvard.edu/>.

## REFERENCES

- Abubekkerov M. K., Antokhina É. A., Cherepashchuk A. M., 2004, *Astronomy Reports*, **48**, 89
- Albrecht S., Reffert S., Snellen I. A. G., Winn J. N., 2009, *nat*, **461**, 373
- Aragona C., McSwain M. V., Grundstrom E. D., Marsh A. N., Roettenbacher R. M., Hessler K. M., Boyajian T. S., Ray P. S., 2009, *apj*, **698**, 514
- Aragona C., McSwain M. V., Becker M. D., 2010, *The Astrophysical Journal*, **724**, 306
- Astropy Collaboration et al., 2013, *aap*, **558**, A33
- Astropy Collaboration et al., 2018, *aj*, **156**, 123
- Astropy Collaboration et al., 2022, *apj*, **935**, 167
- Baba J., Asaki Y., Makino J., Miyoshi M., Saitoh T. R., Wada K., 2009, *apj*, **706**, 471
- Bailer-Jones C. A. L., 2015, *pasp*, **127**, 994
- Bailer-Jones C. A. L., Rybizki J., Fouesneau M., Demleitner M., Andrae R., 2021, *aj*, **161**, 147
- Bikmaev I. F., et al., 2017, *Astronomy Letters*, **43**, 664
- Blauw A., 1961, *bain*, **15**, 265
- Blay P., Negueruela I., Reig P., Coe M. J., Corbet R. H. D., Fabregat J., Tarasov A. E., 2006, *aap*, **446**, 1095
- Brandt N., Podsiadlowski P., 1995, *mnras*, **274**, 461
- Breivik K., et al., 2020a, *apj*, **898**, 71
- Breivik K., et al., 2020b, *apj*, **898**, 71
- Casares J., Ribas I., Paredes J. M., Martí J., Allende Prieto C., 2005a, *mnras*, **360**, 1105
- Casares J., Ribó M., Ribas I., Paredes J. M., Martí J., Herrero A., 2005b, *mnras*, **364**, 899
- Casares J., et al., 2011, in *High-Energy Emission from Pulsars and their Systems*, pp 559–562 ([arXiv:1012.4351](https://arxiv.org/abs/1012.4351)), doi:10.1007/978-3-642-17251-9\_46
- Chaty S., 2013, *Advances in Space Research*, **52**, 2132
- Chen B., et al., 2001, *apj*, **553**, 184
- Densham R. H., Charles P. A., 1982, *mnras*, **201**, 171
- Falanga M., Bozzo E., Lutovinov A., Bonnet-Bidaud J. M., Fetisova Y., Puls J., 2015, *aap*, **577**, A130
- Fortin F., García F., Chaty S., Chassande-Mottin E., Simaz Bunzel A., 2022, *aap*, **665**, A31
- Fryer C. L., Kusenko A., 2006, *apjs*, **163**, 335

<sup>1</sup> <https://github.com/COSMIC-PopSynth/COSMIC>

<sup>2</sup> <http://www.astropy.org>

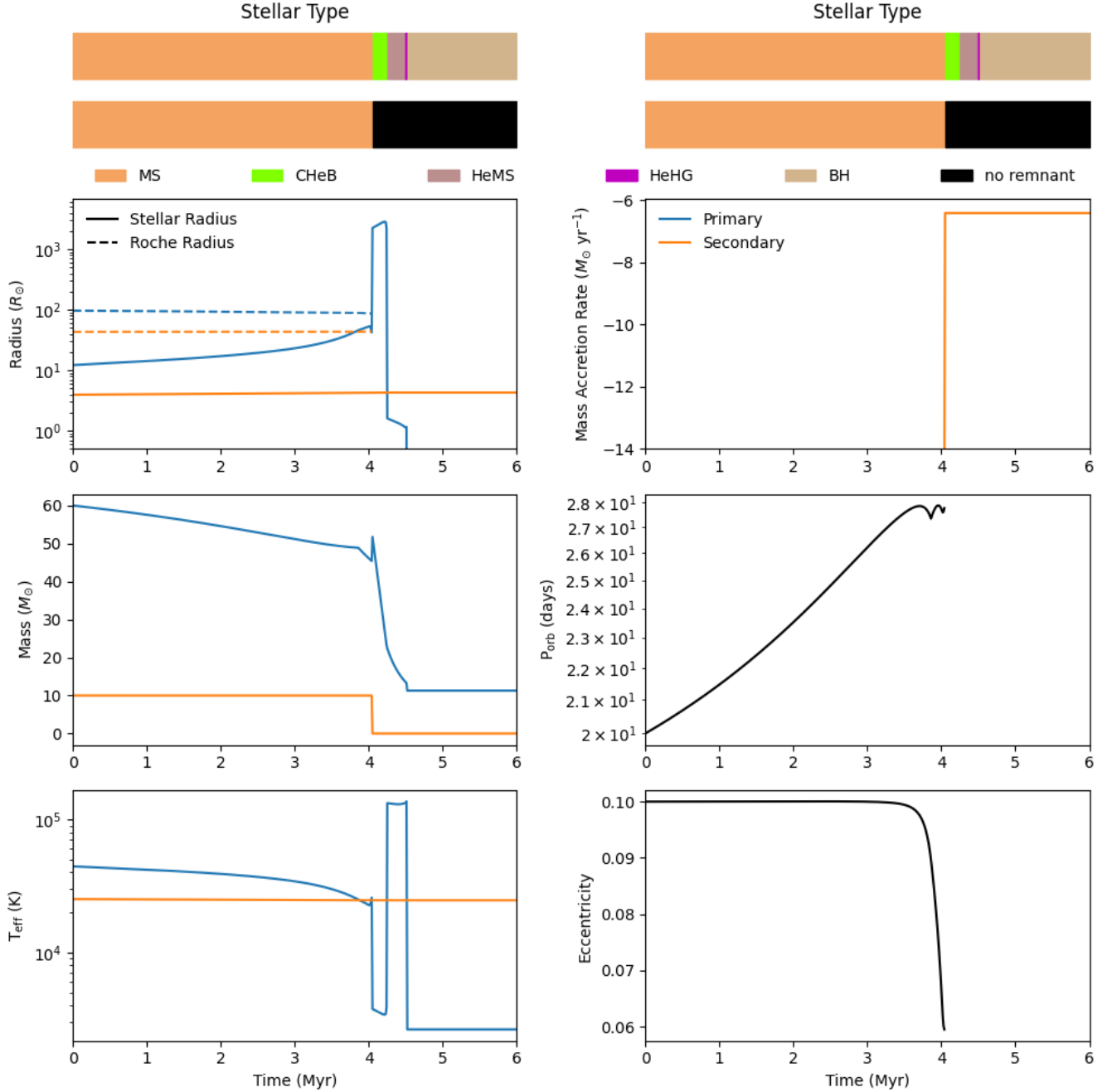


**Figure 23.** Evolution of a binary system. This simulation used the default kick prescription, and the same parameters as the simulations where I varied only the masses, as outlined in section 4.2.1. Here, I used initial masses of  $60M_{\odot}$  and  $10M_{\odot}$  for the progenitor and companion respectively.

Fryer C. L., Belczynski K., Wiktorowicz G., Dominik M., Kalogera V., Holz D. E., 2012, *apj*, 749, 91  
 Gaia Collaboration et al., 2016, *aap*, 595, A1  
 Gaia Collaboration et al., 2022, arXiv e-prints, p. arXiv:2208.00211  
 Gamen R., Barbà R. H., Walborn N. R., Morrell N. I., Arias J. I., Maíz Apellániz J., Sota A., Alfaro E. J., 2015, *aap*, 583, L4  
 Giacobbo N., Mapelli M., 2020, *apj*, 891, 141  
 Gies D. R., Bolton C. T., 1986, *apjs*, 61, 419  
 Grundstrom E. D., et al., 2007, *apj*, 660, 1398  
 Grunhut J. H., Bolton C. T., McSwain M. V., 2014, *aap*, 563, A1  
 Hamers A. S., Samsing J., 2019, *mnr*, 487, 5630

Harris C. R., et al., 2020, *Nature*, 585, 357  
 Heger A., Fryer C. L., Woosley S. E., Langer N., Hartmann D. H., 2003, *apj*, 591, 288  
 Hills J. G., 1975, *aj*, 80, 809  
 Hobbs G., Lorimer D. R., Lyne A. G., Kramer M., 2005, *mnr*, 360, 974  
 Houk N., 1978, Michigan catalogue of two-dimensional spectral types for the HD stars  
 Hu C.-P., Chou Y., Ng C. Y., Lin L. C.-C., Yen D. C.-C., 2017, *apj*, 844, 16  
 Hurley J. R., Tout C. A., Pols O. R., 2002, *mnr*, 329, 897  
 Hutchings J. B., 1984, *pasp*, 96, 312  
 Hutchings J. B., Cowley A. P., Crampton D., Williams G., 1981, *pasp*, 93,

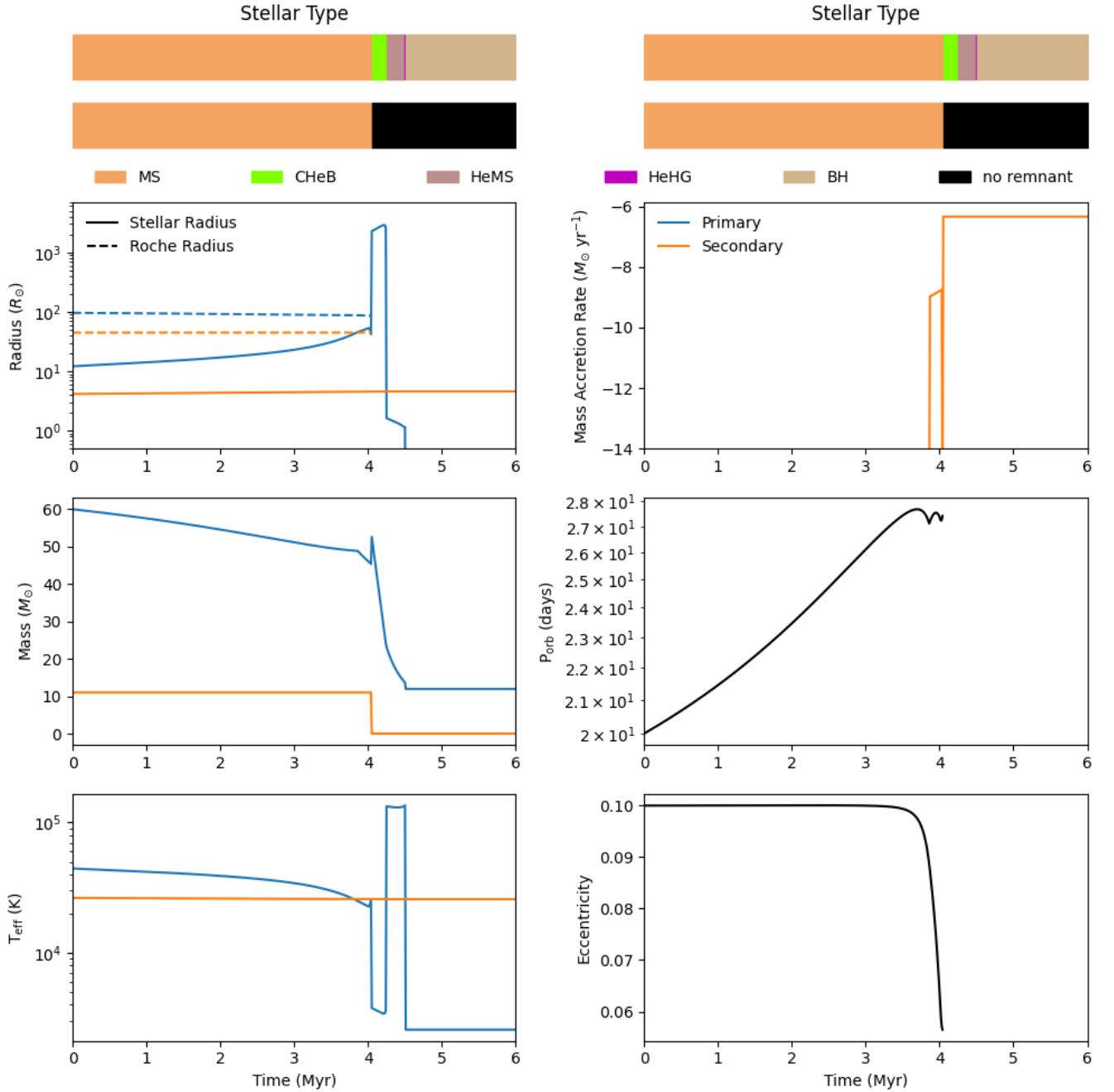


**Figure 24.** Evolution of a binary system. This simulation used the default kick prescription, and the same parameters as the simulations where I varied only the masses, as outlined in section 4.2.1. Here, I used initial masses of  $60M_{\odot}$  and  $11M_{\odot}$  for the progenitor and companion respectively.

741  
Hutchings J. B., Crampton D., Cowley D., Cowley A. P., Bord D. J., 1982, *pasp*, **94**, 541  
Hutchings J. B., Crampton D., Cowley A. P., Thompson I. B., 1987, *pasp*, **99**, 420  
Ivanova N., et al., 2013, *aapr*, **21**, 59  
Jaschek M., Egret D., 1982, *Symposium - International Astronomical Union*, **98**, 261–263  
Justesen A. B., Albrecht S., 2020, *aap*, **642**, A212  
Kaib N. A., Raymond S. N., 2014, *apj*, **782**, 60  
Kaper L., van der Meer A., Najarro F., 2006, *aap*, **457**, 595

Kaplan D. L., Chatterjee S., Gaensler B. M., Anderson J., 2008, *apj*, **677**, 1201  
Kawata D., Bovy J., Matsunaga N., Baba J., 2019, *mnras*, **482**, 40  
Koenigsberger G., Canalizo G., Arrieta A., Richer M. G., Georgiev L., 2003, *rmxaa*, **39**, 17  
Kroupa P., Burkert A., 2001, *The Astrophysical Journal*, **555**, 945  
Krtićka J., Kubát J., Krtićková I., 2015, *aap*, **579**, A111  
Lai D., 2001, in Blaschke D., Glendenning N. K., Sedrakian A., eds., Vol. 578, *Physics of Neutron Star Interiors*. p. 424  
Lyubimkov L. S., Rostopchin S. I., Roche P., Tarasov A. E., 1997, *mnras*, **286**, 549

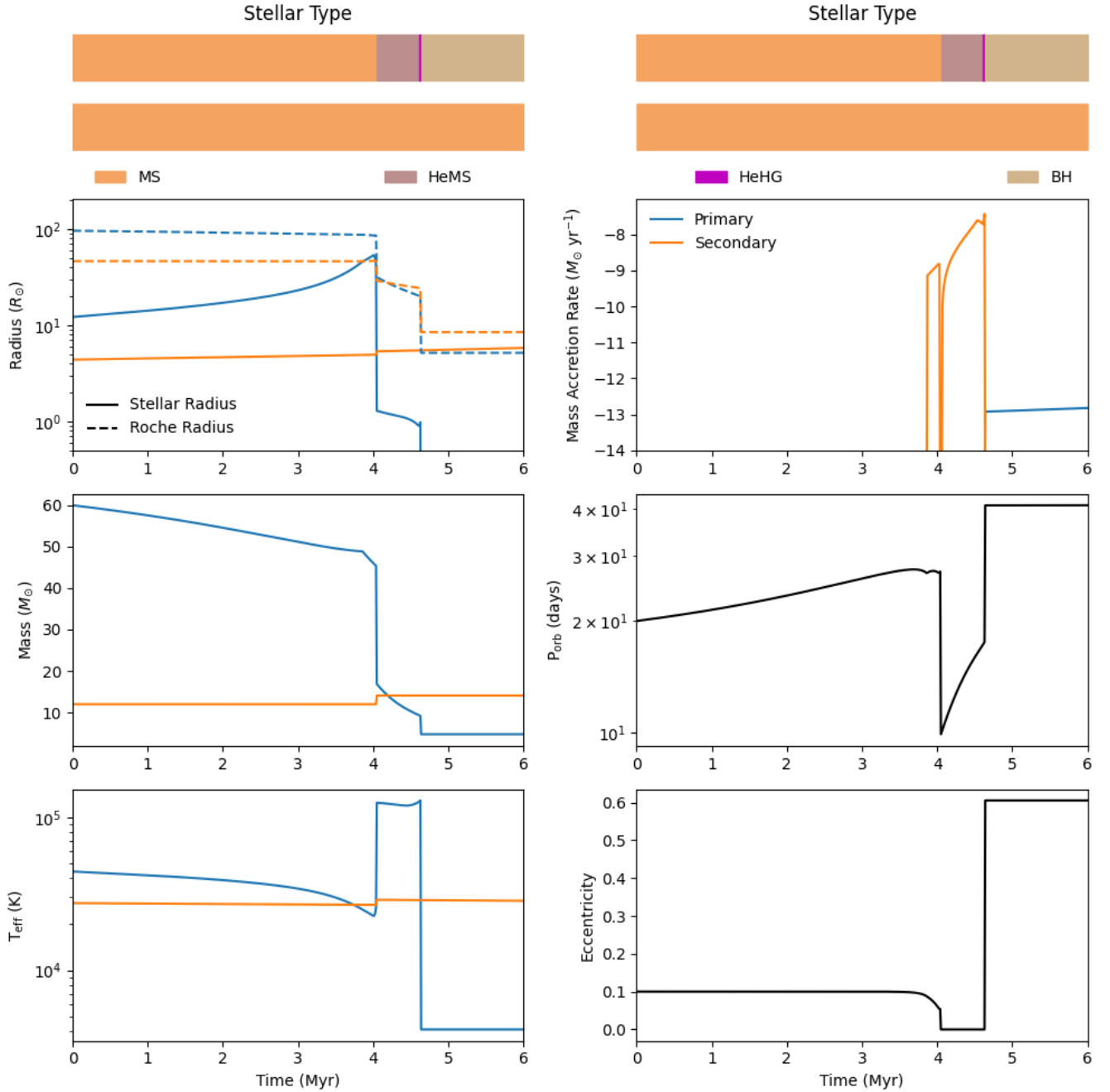


**Figure 25.** Evolution of a binary system. This simulation used the default kick prescription, and the same parameters as the simulations where I varied only the masses, as outlined in section 4.2.1. Here, I used initial masses of  $60M_{\odot}$  and  $12M_{\odot}$  for the progenitor and companion respectively.

Miller-Jones J. C. A., et al., 2018, *mnras*, **479**, 4849  
Moe M., Di Stefano R., 2017, *apjs*, **230**, 15  
Moritani Y., Kawano T., Chimasu S., Kawachi A., Takahashi H., Takata J., Carciofi A. C., 2018, *pasj*, **70**, 61  
Mróz P., et al., 2019, *apjl*, **870**, L10  
Negueruela I., Ribó M., Herrero A., Lorenzo J., Khangulyan D., Aharonian F. A., 2011, *apjl*, **732**, L11  
Ng C. Y., Romani R. W., 2007, *apj*, **660**, 1357  
Nikolaeva E. A., Bikmaev I. F., Melnikov S. S., Galeev A. I., Zhuchkov R. Y., Irtuganov E. N., 2013, *Bulletin Crimean Astrophysical Observatory*, **109**, 27

Okazaki A. T., Negueruela I., 2001, *aap*, **377**, 161  
Parkes G. E., Murrin P. G., Mason K. O., 1978, *mnras*, **184**, 73P  
Pellizza L. J., Chaty S., Negueruela I., 2006, *aap*, **455**, 653  
Reid M. J., et al., 2009, *apj*, **700**, 137  
Reig P., Negueruela I., Papamastorakis G., Manousakis A., Kougentakis T., 2005, *aap*, **440**, 637  
Rivinius T., Carciofi A. C., Martayan C., 2013, *aapr*, **21**, 69  
Sidoli L., Paizis A., 2018, *mnras*, **481**, 2779  
Slettebak A., 1982, *apjs*, **50**, 55  
Sota A., Maíz Apellániz J., Morrell N. I., Barbá R. H., Walborn N. R., Gamen R. C., Arias J. I., Alfaro E. J., 2014, *apjs*, **211**, 10



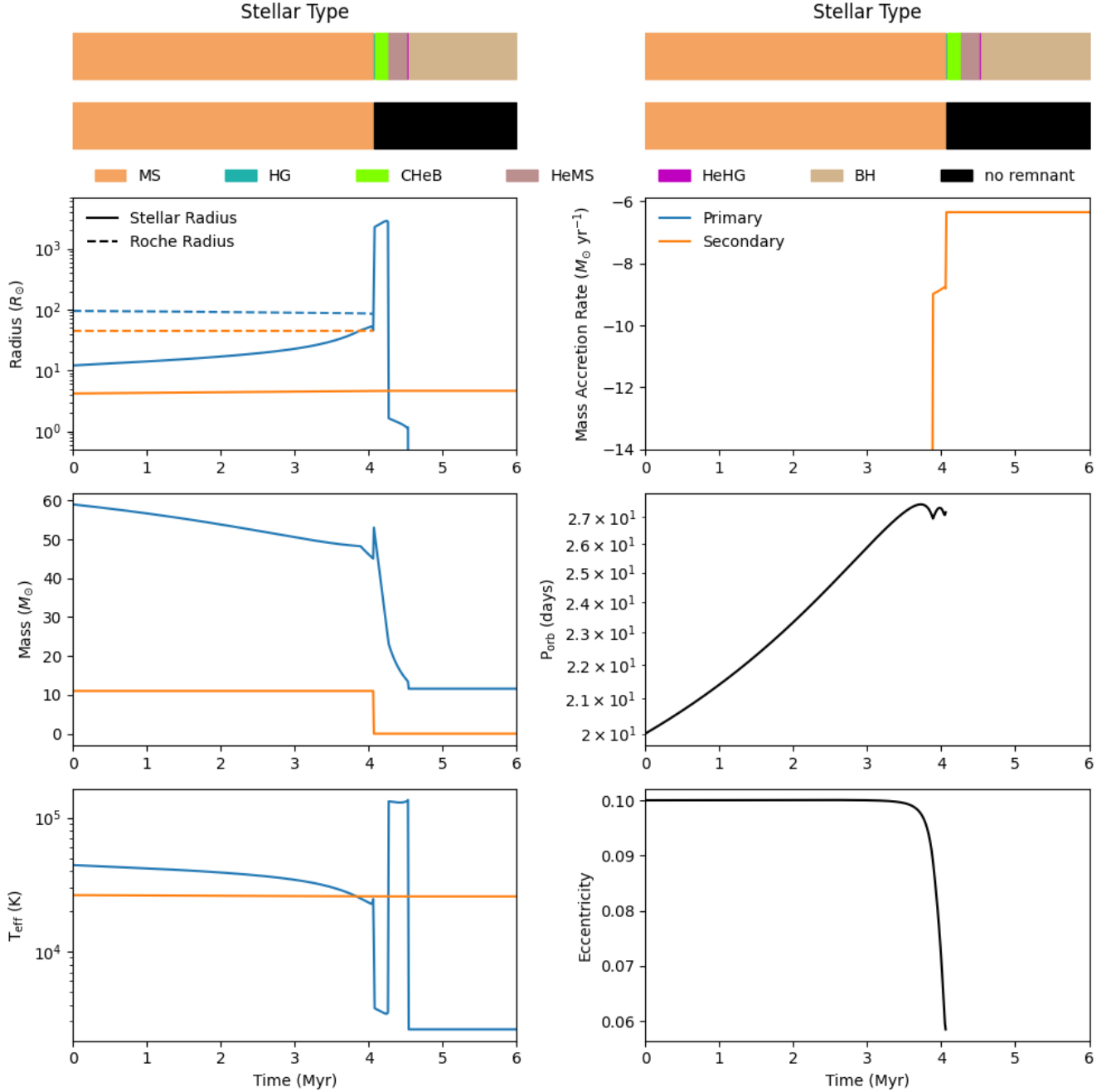


**Figure 26.** Evolution of a binary system. This simulation used the default kick prescription, and the same parameters as the simulations where I varied only the masses, as outlined in section 4.2.1. Here, I used initial masses of  $59M_{\odot}$  and  $11M_{\odot}$  for the progenitor and companion respectively.

Stappers B. W., et al., 2011, *aap*, 530, A80  
 Stickland D., Lloyd C., Radziun-Woodham A., 1997, *mnras*, 286, L21  
 Stoyanov K. A., Zamanov R. K., Latev G. Y., Abedin A. Y., Tomov N. A., 2014, *Astronomische Nachrichten*, 335, 1060  
 Sukhbold T., Ertl T., Woosley S. E., Brown J. M., Janka H. T., 2016, *apj*, 821, 38  
 Townsend L. J., Coe M. J., Corbet R. H. D., Hill A. B., 2011, *mnras*, 416, 1556  
 Valtonen M. J., 1997, *apj*, 485, 785  
 Walch S., Naab T., 2015, *Monthly Notices of the Royal Astronomical Society*, 451, 2757

Wang Z. X., Gies D. R., 1998, *pasp*, 110, 1310  
 Wang C., Lai D., Han J. L., 2006, *apj*, 639, 1007  
 Wenger M., et al., 2000, *aaps*, 143, 9  
 Wes McKinney 2010, in Stéfan van der Walt Jarrod Millman eds, Proceedings of the 9th Python in Science Conference. pp 56 – 61, doi:10.25080/Majora-92bf1922-00a  
 Zorec J., Frémat Y., Cidale L., 2005, *aap*, 441, 235  
 pandas development team T., 2020, pandas-dev/pandas: Pandas, doi:10.5281/zenodo.3509134, <https://doi.org/10.5281/zenodo.3509134>  
 van den Heuvel E. P. J., Portegies Zwart S. F., Bhattacharya D., Kaper L.,

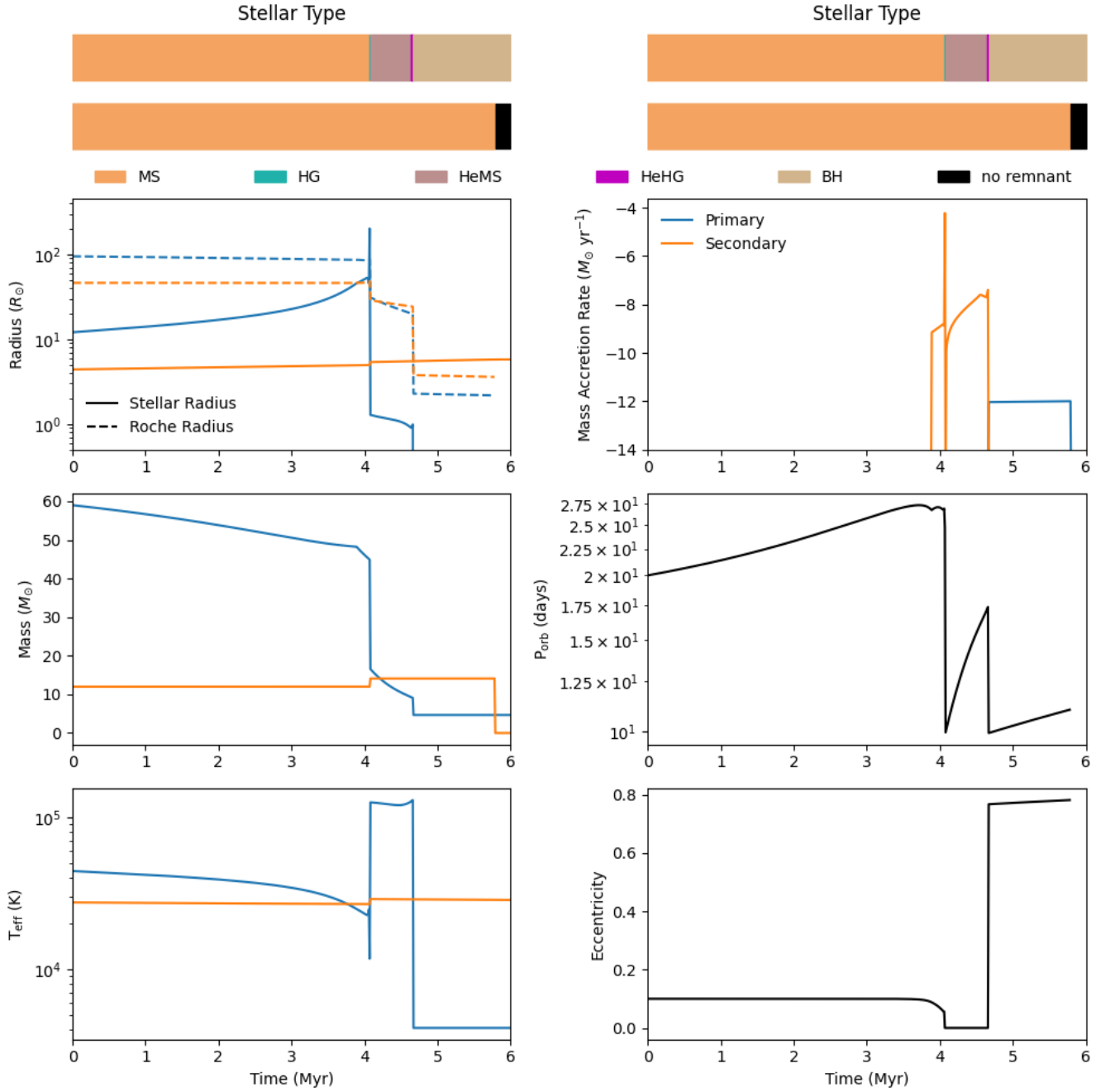


**Figure 27.** Evolution of a binary system. This simulation used the default kick prescription, and the same parameters as the simulations where I varied only the masses, as outlined in section 4.2.1. Here, I used initial masses of  $59M_{\odot}$  and  $12M_{\odot}$  for the progenitor and companion respectively.

2000, *aap*, 364, 563

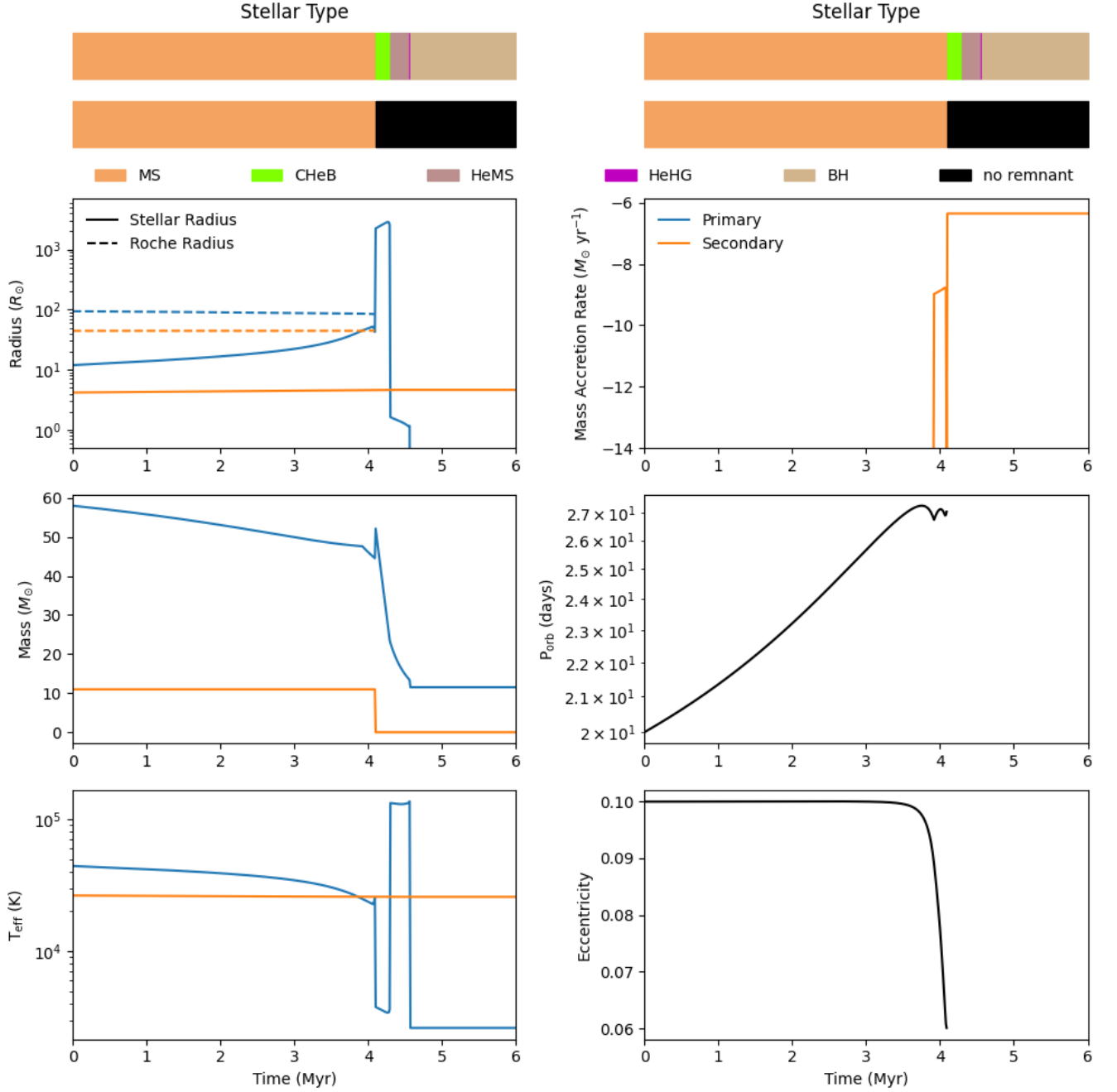


**Figure 28.** Evolution of a binary system. This simulation used the default kick prescription, and the same parameters as the simulations where I varied only the masses, as outlined in section 4.2.1. Here, I used initial masses of  $58M_{\odot}$  and  $11M_{\odot}$  for the progenitor and companion respectively.

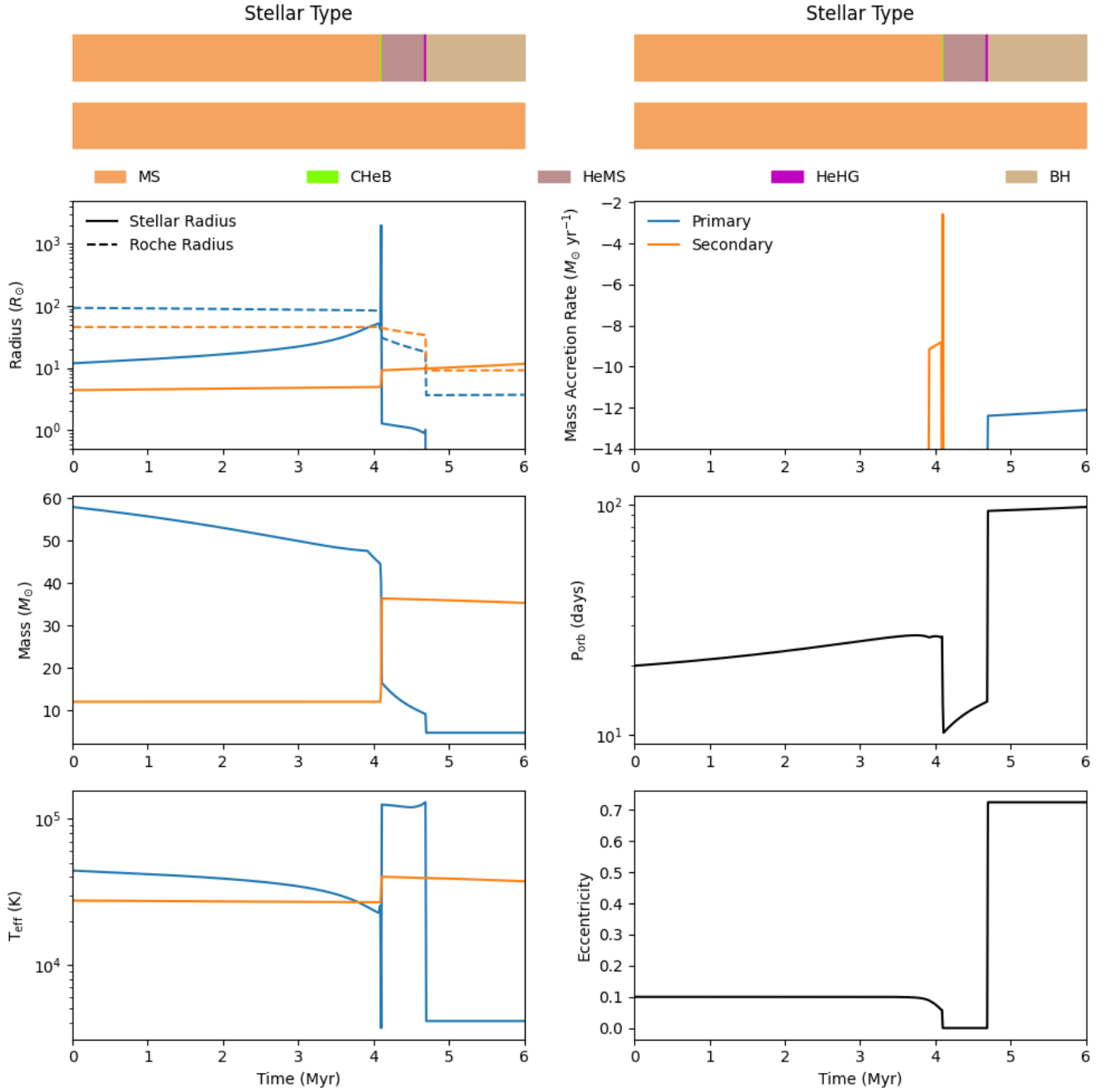


**Figure 29.** Evolution of a binary system. This simulation used the default kick prescription, and the same parameters as the simulations where I varied only the masses, as outlined in section 4.2.1. Here, I used initial masses of  $58M_{\odot}$  and  $12M_{\odot}$  for the progenitor and companion respectively.

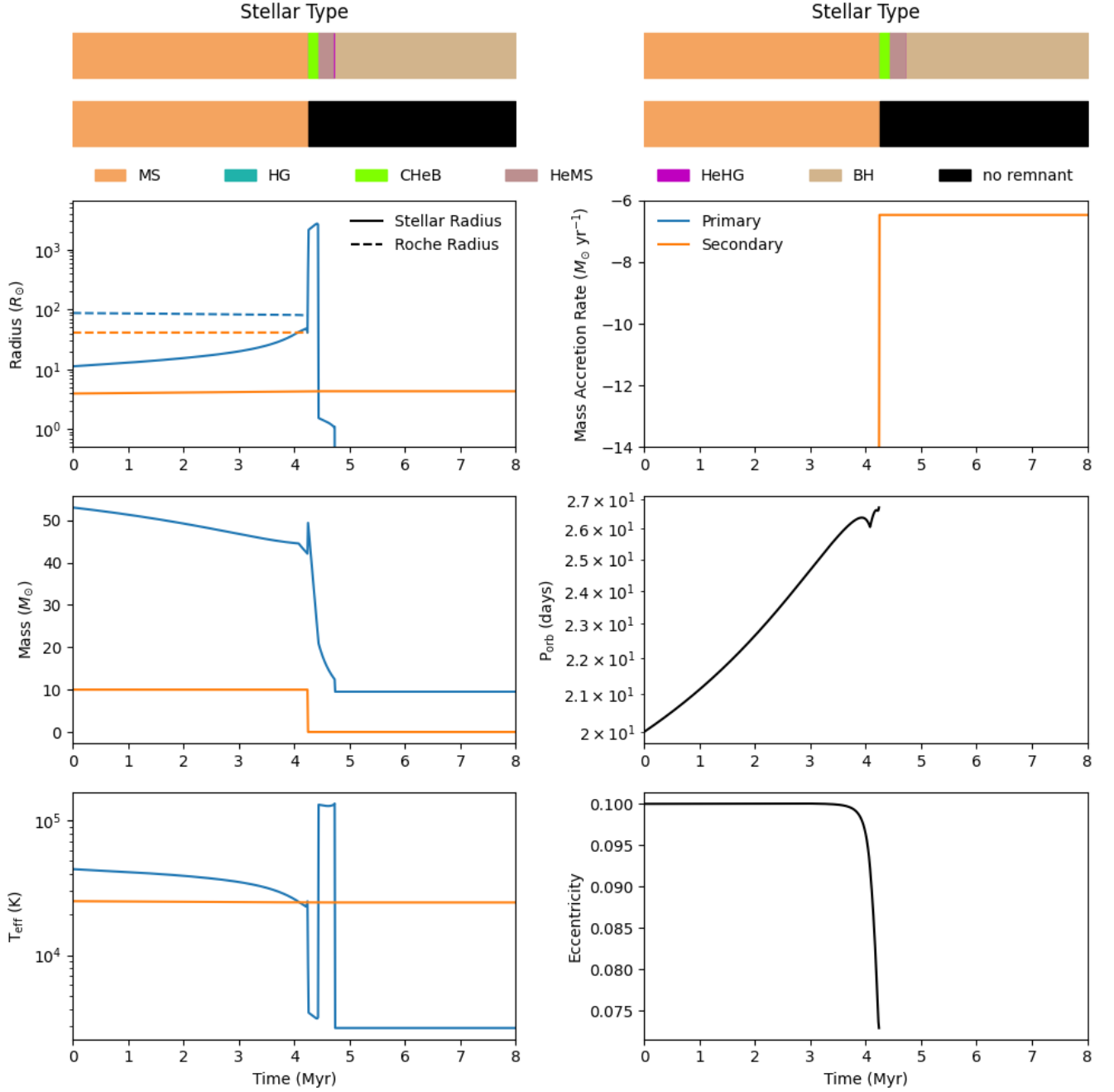


**Figure 30.** Evolution of a binary system. This simulation used the default kick prescription, and the same parameters as the simulations where I varied only the masses, as outlined in section 4.2.1. Here, I used initial masses of  $53M_\odot$  and  $10M_\odot$  for the progenitor and companion respectively.



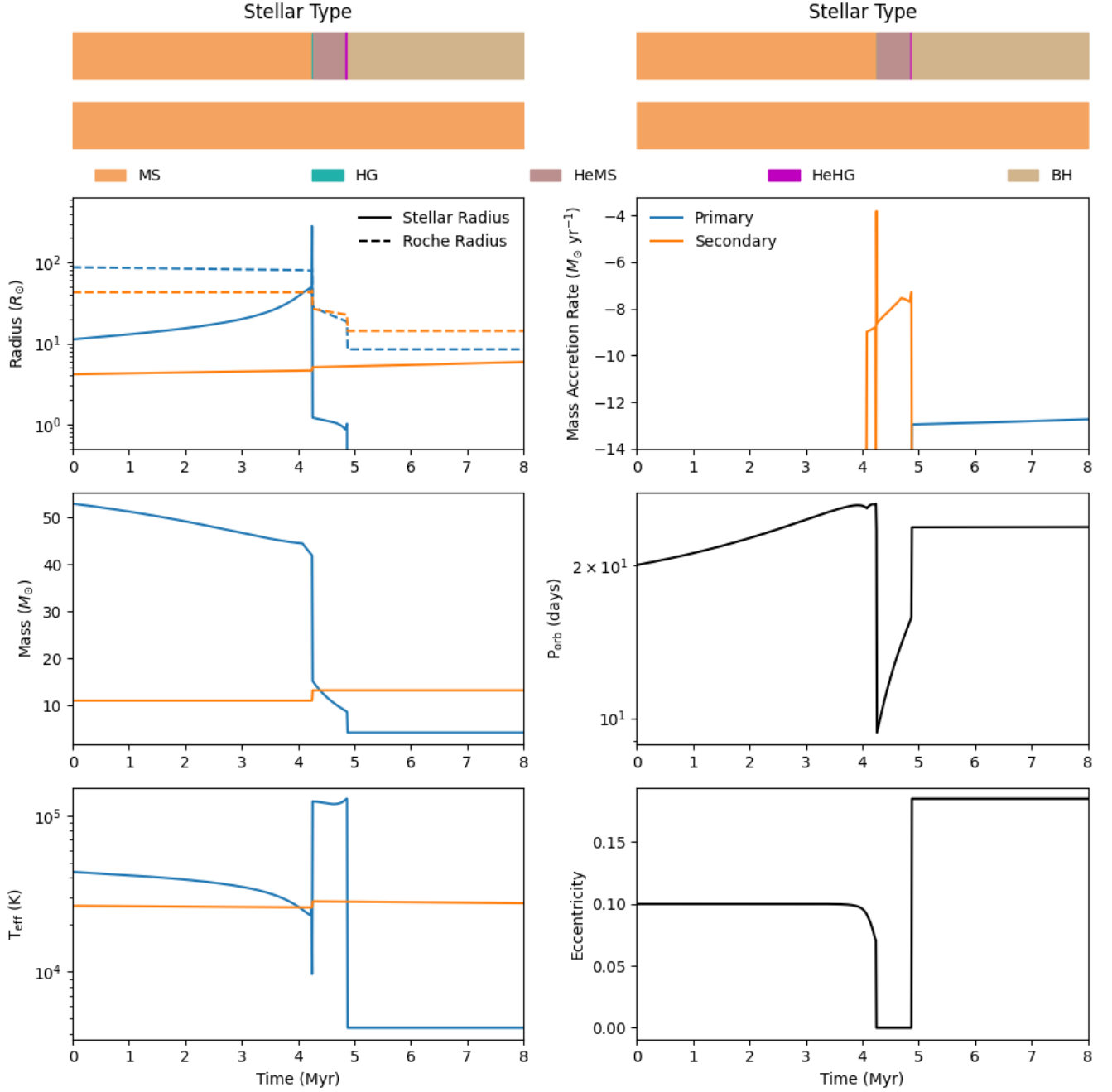


**Figure 31.** Evolution of a binary system. This simulation used the default kick prescription, and the same parameters as the simulations where I varied only the masses, as outlined in section 4.2.1. Here, I used initial masses of  $53M_{\odot}$  and  $11M_{\odot}$  for the progenitor and companion respectively.

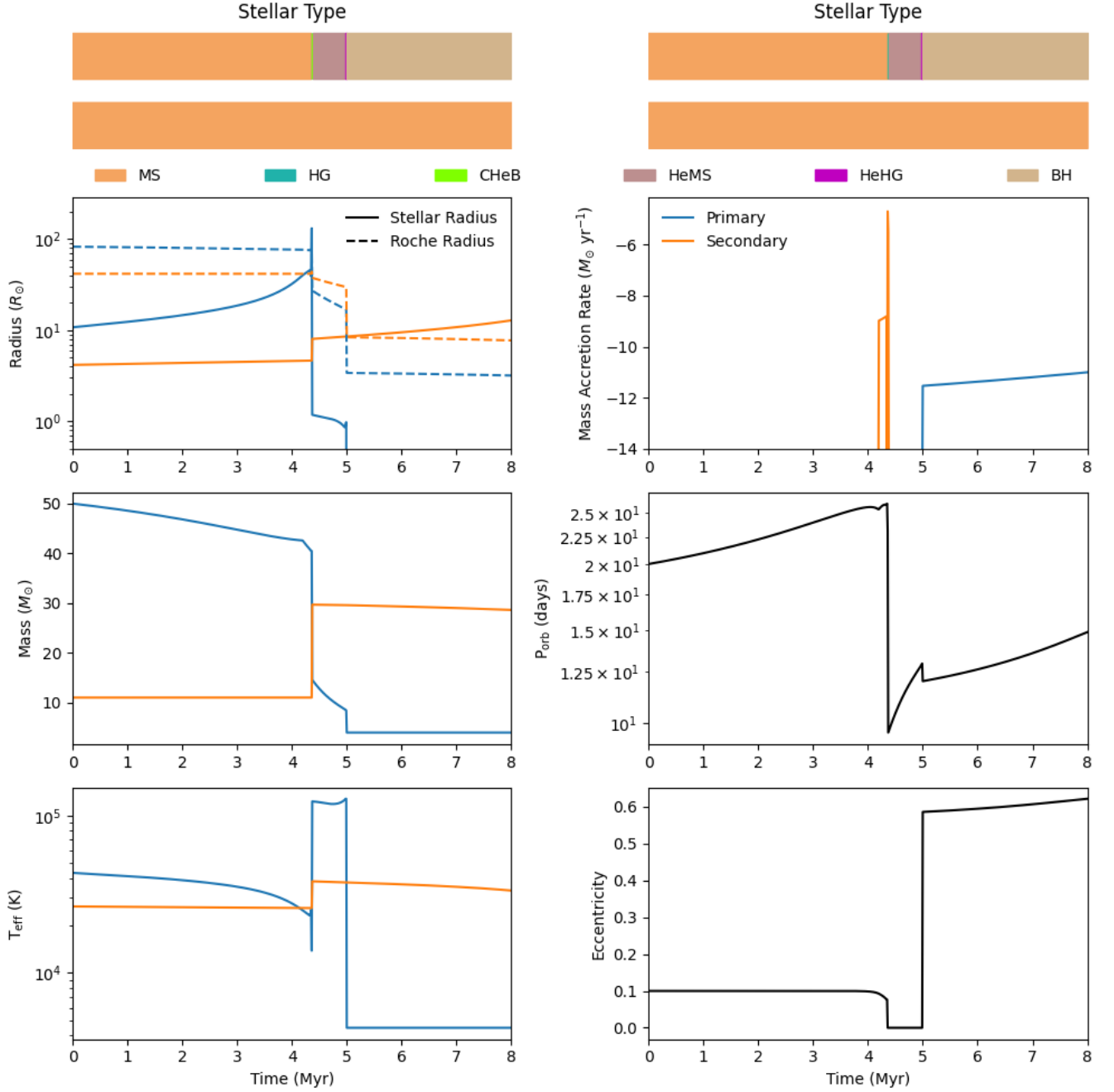


**Figure 32.** Evolution of a binary system. This simulation used the default kick prescription, and the same parameters as the simulations where I varied only the masses, as outlined in section 4.2.1. Here, I used initial masses of  $50M_{\odot}$  and  $11M_{\odot}$  for the progenitor and companion respectively.

**APPENDIX A: QUERYING GAIA**

The query below was used to select the required data from *Gaia* -

```
SELECT gaia.source_id, ra, ra_error, dec,
dec_error, parallax, parallax_error, pmra,
pmra_error, pmdec, pmdec_error FROM ga-
iadr3.gaia_source AS gaia INNER JOIN
user_hjohnson.peculiarvelocitysourceid ON
gaia.source_id =
user_hjohnson.peculiarvelocitysourceid.source_id
Where hjohnson.peculiarvelocitysourceid is my table
with the source IDs.
```

**APPENDIX B: CALCULATING PECULIAR VELOCITIES**

The following table gives descriptions, names, and values/units where appropriate for all the quantities used for the following calculation. Unit conversions (eg, parsecs to kilometres) are not explicitly shown.

I first used Astropy to convert from Ra and Dec coordinates to galactic coordinates,  $l$  (galactic longitude) and  $b$  (galactic latitude) using the quantities  $v_\odot$ ,  $v_{lsr}$ ,  $R_\odot$ , and  $z_{sun}$  shown in table B1. This gives me the velocity vector for the sources including motions due to the sun -  $\vec{v}_{source} = (U_1, V_1, W_1)$ .

Next, I calculate the distance to the source using parallax inversion -

$$D = \frac{1}{\pi} \quad (B1)$$

Now, I calculate the distance of the source from the Sun in the galactic plane -

$$D_p = D \cos(b) \quad (B2)$$

Next, calculate the distance of the source from the centre of the galaxy -

$$R_p^2 = R_\odot^2 + D_p^2 - 2R_\odot D_p \cos(l) \quad (B3)$$

The angle between the source and the Sun as viewed from the galactic centre is given by -

$$\sin(\beta) = \frac{D_p \sin(l)}{R_p} \quad (B4)$$

$$\cos(\beta) = \frac{R_\odot - D_p \cos(l)}{R_p} \quad (B5)$$

I then rotate the galactocentric velocity vector  $\vec{v}_{source}$  components through the angle  $\beta$  and remove the galactic rotation velocity -

$$U_2 = U_1 \cos(\beta) - V_1 \sin(\beta) \quad (B6)$$

$$V_2 = V_1 \cos(\beta) + U_1 \sin(\beta) - v_{lsr} \quad (B7)$$

$$W_2 = W_1 \quad (B8)$$

The vector  $(U_2, V_2, W_2)$  gives the peculiar motion of the source in the galactocentric frame.  $U_2$  is radially inwards towards the galactic centre from the point of view of the source,  $V_2$  is in the direction of galactic rotation at the source, and  $W_2$  is directed towards the north

galactic pole.

The final step for the magnitude of peculiar velocity is simply Pythagorean velocity addition -

$$V_{tot} = \sqrt{U_2^2 + V_2^2 + W_2^2} \quad (B9)$$

This paper has been typeset from a  $\text{\LaTeX}$  file prepared by the author.

**Table B1.** Useful quantities and their definitions for the calculation of peculiar velocities.

Quantity Name	Description	Value/unit
$l$	Galactic Longitude	Degrees
$b$	Galactic Latitude	Degrees
$\vec{v}_{\odot}$	Solar velocity	$(8.0, 12.4, 7.7) \text{ kms}^{-1}$
$v_{lsr}$	Galactic rotation speed	$236 \text{ kms}^{-1}$
$R_{\odot}$	Distance from Sun to galactic centre	8.2 kpc
$z_{sun}$	Height of Sun above galactic plane	27 pc
$D$	Distance to source	pc
$\pi$	Parallax	arcsec
$D_p$	Distance of source from Sun projected in galactic plane	km
$R_p$	Distance of source from galactic centre projected in galactic plane	km
$\beta$	Angle between source and Sun as viewed from the galactic centre	Degrees
$\vec{v}_{source}$	Velocity vector of the source including galactic motion	$(U_1, V_1, W_1) \text{ kms}^{-1}$
$V_{tot}$	Magnitude of peculiar velocity of the source	$\text{kms}^{-1}$